Remote Sensing of Environment 269 (2022) 112810

Contents lists available at ScienceDirect

Remote Sensing of Environment

journal homepage: www.elsevier.com/locate/rse

Quantifying latitudinal variation in land surface phenology of *Spartina alterniflora* saltmarshes across coastal wetlands in China by Landsat 7/8 and Sentinel-2 images

Xi Zhang [a], Xiangming Xiao [b,*], Shiyun Qiu [a], Xiao Xu [a], Xinxin Wang [a], Qing Chang [c], Jihua Wu [a], Bo Li [a,d,**]

[a] Ministry of Education Key Laboratory of Biodiversity Science and Ecological Engineering, National Observations and Research Station for Wetland Ecosystems of the Yangtze Estuary, Institute of Biodiversity Science and Institute of Eco-Chongming, School of Life Sciences, Fudan University, Shanghai 200438, China
[b] Department of Microbiology and Plant Biology, Center for Earth Observation and Modeling, University of Oklahoma, Norman, OK 73019, USA
[c] Indiana University, School of Public and Environmental Affairs, Bloomington, Indiana 47405, USA
[d] Centre for Invasion Biology, Institute of Biodiversity, Yunnan University, Kunming, Yunnan 650504, China

ARTICLE INFO

Editor: Marie Weiss

Keywords:
Spartina alterniflora
Coastal saltmarshes
Plant invasions
Land surface phenology
Latitudinal variation
Accumulated growing degree-days
Ecosystem management

ABSTRACT

Spartina alterniflora is an aggressive invasive plant spreading along the coastal China, spanning a latitudinal range of 20°N - 39°N, and its invasion resulted in dramatic decline in both native plant diversity and ecosystem functioning. Phenology of *S. alterniflora* saltmarshes is a critical feature to elucidate the invasion dynamics over geographical regions but has not been well understood yet. In this study, we examined the variation of *S. alterniflora* saltmarsh phenology across coastal China during 2018–2020 by using time series Landsat 7/8 and Sentinel-2 images. Combined Landsat 7/8 and Sentinel-2 images provided more good-quality observations in a year, which could facilitate phenological retrieval. We applied and assessed three widely used phenology retrieval methods (i.e., NDVI-based pixel-specific statistical threshold, NDVI-based double logistic mathematical equation, and LSWI-based biological threshold) for retrieving the start and end of season (SOS and EOS) as well as the length of season (LOS) of *S. alterniflora* saltmarshes. The SOS and EOS dates derived from three phenology retrieval methods showed similar patterns in latitudinal phenology variation: SOS became later and LOS became shorter as latitude increased, and the latitudinal trend of EOS was not as large as that of SOS. This study shows the potential of Landsat 7/8 and Sentinel-2 to quantify land surface phenology of *S. alterniflora* saltmarshes, which not only enhances our understanding of the spatial-temporal dynamics of coastal saltmarshes in China but also improves the management of this plant invader that threatens native saltmarshes in the world.

1. Introduction

Plant phenology is the timing of seasonal developmental stages in plant life cycles, which is an important indicator for climate change, land cover change, and agriculture production (Bolton and Friedl, 2013; Bórnez et al., 2020; Piao et al., 2019; Zhong et al., 2014). Recently, the role of phenology in plant invasions has been increasingly recognized (Wolkovich and Cleland, 2014). Some studies have found that in comparison with native species, invasive species have distinct phenological traits, for example, earlier emergence, later senescence, or both, which often result in longer growth period (Fridley, 2012; Liao et al., 2007). This extended phenology is considered as a temporal niche for invasive species to assimilate resources both in spring and autumn (Wolkovich and Cleland, 2011), which facilitates invasive species to establish and gain competitive advantage. In addition, several studies have reported that invasive species respond more sensitively to climate warming by adjusting their phenology (e.g., earlier flowering) than native species (Esch et al., 2019; Willis et al., 2010; Zettlemoyer et al., 2019), which

* Corresponding author at: Department of Microbiology and Plant Biology, Center for Earth Observation and Modeling, University of Oklahoma, Norman, OK 73019, USA.
** Corresponding author at: Ministry of Education Key Laboratory of Biodiversity Science and Ecological Engineering, National Observations and Research Station for Wetland Ecosystems of the Yangtze Estuary, Institute of Biodiversity Science and Institute of Eco-Chongming, School of Life Sciences, Fudan University, Shanghai 200438, China; and Centre for Invasion Biology, Institute of Biodiversity, Yunnan University, Kunming, Yunnan 650504, China.
E-mail addresses: xiangming.xiao@ou.edu (X. Xiao), bool@fudan.edu.cn (B. Li).

https://doi.org/10.1016/j.rse.2021.112810
Received 22 April 2021; Received in revised form 12 November 2021; Accepted 16 November 2021
Available online 23 November 2021

also exacerbates the invasion processes in the context of global warming. It has been acknowledged that most of exotic species tend to invade large geographic areas and diverse habitats (Turbelin et al., 2017), but few studies have investigated the phenology change of invasive species along the environmental gradients.

Hot spots of plant invasions are found on islands or in coastal regions like saltmarshes (Dawson et al., 2017; Mark et al., 2018). In 1979, *Spartina alterniflora* (hereafter, *S. alterniflora*), a perennial grass native to the Atlantic and Gulf Coasts of North America, was first introduced to China for tidal reclamation and erosion mitigation. Since then, it has rapidly invaded the areas from north to south (20°N - 39°N) across coastal wetlands of China (Xu et al., 2020a; Zuo and Zhao, 2012). Over the past decades, many researchers have studied several traits of *S. alterniflora* across the latitudes in its native and introduced regions through field surveys or common garden experiments, such as stem height and diameter (Liu et al., 2016a; Shang et al., 2015), seed set and production (Liu et al., 2020c), and productivity (Kirwan et al., 2009; Liu et al., 2020b; Wieski and Pennings, 2014). These studies have led us to deduce whether the rapid spread of *S. alterniflora* over a wide range of environmental conditions in China is reached by phenotype plasticity or evolutionary adaptation. As an integrative indicator, the phenological trait, especially for leaf emergence and senescence, of *S. alterniflora* along the latitudinal gradient remains poorly understood. Several studies have reported phenology information of *S. alterniflora* at one or few selected locations from in-situ observations or satellite derivations (Ai et al., 2017; Qiu et al., 2018; Sun et al., 2016; Wu et al., 2020; Zhang et al., 2020), however, those phenometrics estimates were from different data sources or different phenology algorithms and could not be compared on a latitudinal basis.

Phenological metrics could be derived from ground observations, phenology modeling, and satellite images (Piao et al., 2019). Ground observations provide specific and accurate timing of plant phenophases but cannot cover continuously large regions (Garrity et al., 2011). From a remote sensing perspective, land surface phenology (LSP) describes the spatio-temporal development of the vegetated land surface as revealed by synoptic space-borne sensors (White et al., 2009). Many efforts have been made to study phenology from satellite data in a variety of terrestrial and aquatic environments, such as forests (Garrity et al., 2011; Melaas et al., 2013), grasslands (Shen et al., 2016; Shen et al., 2011), farmlands (Bolton and Friedl, 2013; Huang and Zhu, 2019), and phytoplankton communities (Palmer et al., 2015), but satellite-based phenology study of coastal saltmarshes remain limited (Ghosh and Mishra, 2017). Coastal saltmarshes are generally narrow belts, the monitoring of which requires satellite images with high spatial resolution. Time series Landsat images (30-m spatial resolution, 16-day temporal resolution) are widely used to obtain LSP information (Dong et al., 2016; Liu et al., 2020a). However, the use of Landsat images for phenology research often has two limitations: (1) some phenological transitions occur more rapidly than the 16-day repeat cycle of Landsat, and (2) cloud and cloud shadow reduce the number of good-quality observations available for identifying phenological events. Newly available imagery from Sentinel-2A/B (10-m or 20-m spatial resolution, 5-day temporal resolution), in combination with Landsat images, can partially overcome this constraint.

A number of studies have reported various ways to understand satellite-derived SOS (start of season) and EOS (end of season) dates, including climate data (de Beurs and Henebry, 2005; Zhang et al., 2004), bioclimatic models (Schwartz and Reed, 1999), and in-situ phenology observations (Fisher and Mustard, 2007; Garrity et al., 2011). Because the available in-situ phenology data sources are limited and leaf-on (SOS) and leaf-off (EOS) in the temperate zone are driven by temperature, many studies used air temperature, growing degree days, and other temperature-related variables to analyze the relationship between temperature and satellite-based SOS and EOS estimates (Reed et al., 2009). For example, some studies have shown that plant phenology described by time series vegetation indices can be well approximated as a quadratic function of thermal time (de Beurs and Henebry, 2004; Krehbiel et al., 2017), from which the fitted curve of vegetation indices can be used to alternatively derive phenological metrics (Nguyen et al., 2020). Other studies have indicated that remote sensing-based surface temperature (i.e., land surface temperature, LST) correlated well with canopy greenness dynamics as observed from vegetation indices in most terrestrial ecosystems, and was also a good proxy for estimating SOS and EOS (Dong et al., 2015; Hassan and Rahman, 2012; Liu et al., 2016b). For coastal ecosystems, apart from land surface temperature, plant leaf emergence, growth, and senescence are inevitably influenced by sea surface temperature (SST) (Egan and Ungar, 1999). Although many studies have revealed the strong correlations between LST and LSP for terrestrial vegetation (Han and Xu, 2013; Xu et al., 2020b), the relationships between LST, SST, and LSP for coastal vegetation along the latitudes are poorly understood.

In this study, the following three questions were addressed: (1) What are the differences in SOS and EOS of *S. alterniflora* saltmarshes retrieved from the three phenology retrieval methods with combined Landsat 7/8 and Sentinel-2 images? (2) What are the temperature conditions of SOS and EOS dates from various phenology retrieval methods, depicted by air temperature (AirT), sea surface temperature (SST), and land surface temperature (LST)? (3) How do the SOS and EOS of *S. alterniflora* saltmarshes vary along the latitudinal gradient across coastal China? We first retrieved and compared phenological metrics by using three phenology retrieval methods and combined Landsat/Sentinel images. In order to assess the retrieved phenological metrics, air temperature data from a reanalysis climate dataset, sea surface temperature data from AVHRR, and land surface temperature data from MODIS were used to analyze the relationships between temperature conditions and phenological metrics. We assumed that the phenological retrievals are reasonable when they agree well with temperature conditions indicated by accumulated growing degree-days (AGDD) at SOS dates and mean temperature at EOS dates. Then we examined the latitudinal variation of *S. alterniflora* saltmarsh phenology across the coastal regions of China. By conducting a large-scale study on phenology of *S. alterniflora* saltmarshes, this study could shed lights not only on the mechanisms of *S. alterniflora* invasion that are essential to its management, but also on the prediction of future invasion dynamics. Moreover, monitoring of *S. alterniflora* saltmarsh phenology with high accuracy is also crucial for the studies of carbon, water, and surface energy fluxes of coastal saltmarshes.

2. Materials and methods

2.1. Study area

The study area is located in the coastal zone of mainland China including eight provinces or municipalities (Hebei, Tianjin, Shandong, Jiangsu, Shanghai, Zhejiang, Fujian, and Guangxi) and ranges from 20°10′N to 40°0′N. Because Liaoning and Guangdong provinces have relatively small continuous areas of *S. alterniflora* saltmarshes, we did not consider *S. alterniflora* saltmarshes in these two provinces in this study (Fig. 1). This region covers the temperate zone, subtropical zone, and tropical zone from north to south. Since the end of the 1970s, *S. alterniflora* has been introduced into many intertidal areas in China and become the most dominant species in the coastal saltmarshes. Several estuaries and bays such as Yellow River estuary, Yangtze estuary, and Luoyuan bay are the hot-spots of *S. alterniflora* invasions.

2.2. Data and processing

2.2.1. Landsat 7/8 and Sentinel-2 data

In this study we used Landsat Collection 2 Level-2 surface reflectance (SR) data and Sentinel-2 Level-2A (SR) data archived in Google Earth Engine (GEE) cloud platform from January 1, 2018 to January 1, 2021. Landsat data include all available Landsat 7 Enhanced Thematic Mapper

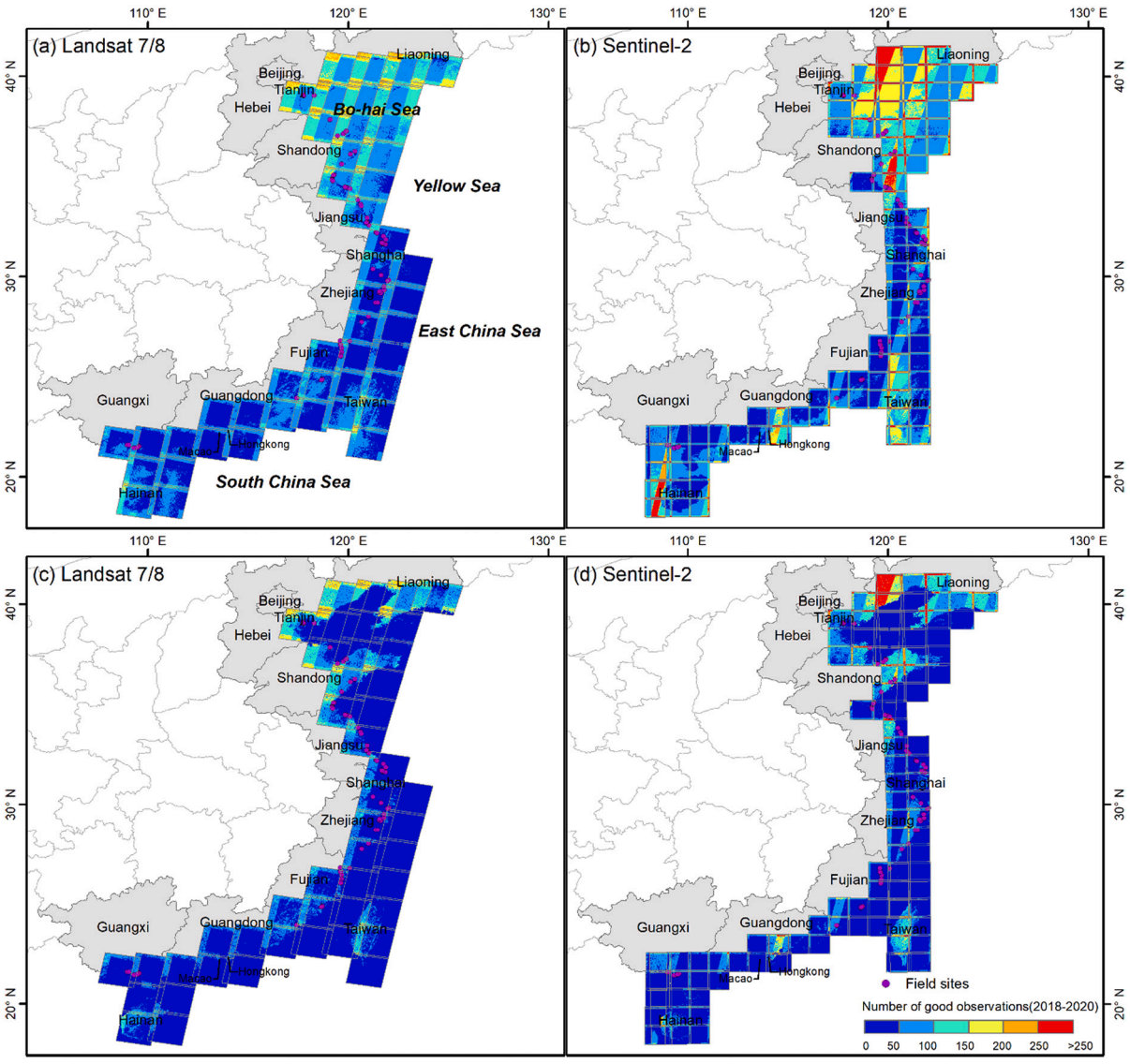

Fig. 1. Location of study area and availability of Landsat 7/8 and Sentinel-2 images from 2018 to 2020 after applying cloud mask (a, b) and cloud and inundation mask (c, d).

(ETM+) and Landsat 8 Operational Land Imager (OLI) images from the United States Geological Survey (USGS). Sentinel-2 data include all available Sentinel-2A and Sentinel-2B Multi Spectral Instrument (MSI) images from the European Space Agency (ESA). Landsat has 16-day revisit cycle, and Landsat 7/8 images together have 8-day temporal resolution. Sentinel-2 has 10-day revisit cycle, and Sentinel-2A/B images together have 5-day temporal resolution. Landsat 7/8 and Sentinel-2 SR products are radiometrically and geometrically corrected.

The data preprocessing included four steps: (1) identifying bad-quality observations, (2) harmonizing Landsat and Sentinel images, (3) calculating vegetation indices, and (4) constructing time series datasets. The first three steps were conducted in the GEE platform and the last step was processed in R software (R Core Team, 2013).

The quality of Landsat 7/8 and Sentinel-2 SR data was assessed based on the quality assessment band (QA_PIXEL) and s2cloudless algorithm, respectively. All bad-quality observations including clouds, cloud shadows, cirrus, and snow/ice were identified in Landsat 7/8 collection. Clouds were identified from the Sentinel-2 cloud probability dataset (s2cloudless) and shadows were defined by cloud projection intersection with low-reflectance near-infrared (NIR) pixels. Fig. 1 shows the spatial distributions of the number of good-quality observations at the pixel scale from Landsat 7/8 and Sentinel-2 datasets during 2018–2020. Fig. 2 shows the number of observations for selected *S. alterniflora* saltmarsh ROIs from Landsat 7/8 and Sentinel-2 datasets during 2018–2020.

In order to increase the number of good-quality observations for identifying phenology (SOS, EOS) of saltmarshes, we harmonized and combined Landsat ETM+, OLI, and Sentinel MSI images. Due to the differences in band wavelengths from these three sensors, we firstly transformed the spectral bands of Landsat 7 ETM+ and Sentinel-2 MSI to match those of Landsat 8 OLI by using the linear correction methods proposed by Roy et al. (2016) and Zhang et al. (2018). Two types of regression analyses were conducted by Roy et al. (2016) and Zhang et al. (2018) including ordinary least square (OLS) regression and reduced major axis (RMA) regression, and we used the OLS transformation coefficients in this study. Then we merged these three datasets by their acquisition time and constructed a comparable time series dataset (i.e., combined Landsat/Sentinel images). The combined Landsat/Sentinel time series data has at least one observation within a 5-day period, which facilitates following data compositing.

We calculated three vegetation indices (Normalized Difference Vegetation Index, NDVI, Enhanced Vegetation Index, EVI, and Land Surface Water Index, LSWI) using Eqs. (1)–(3). The intertidal areas are

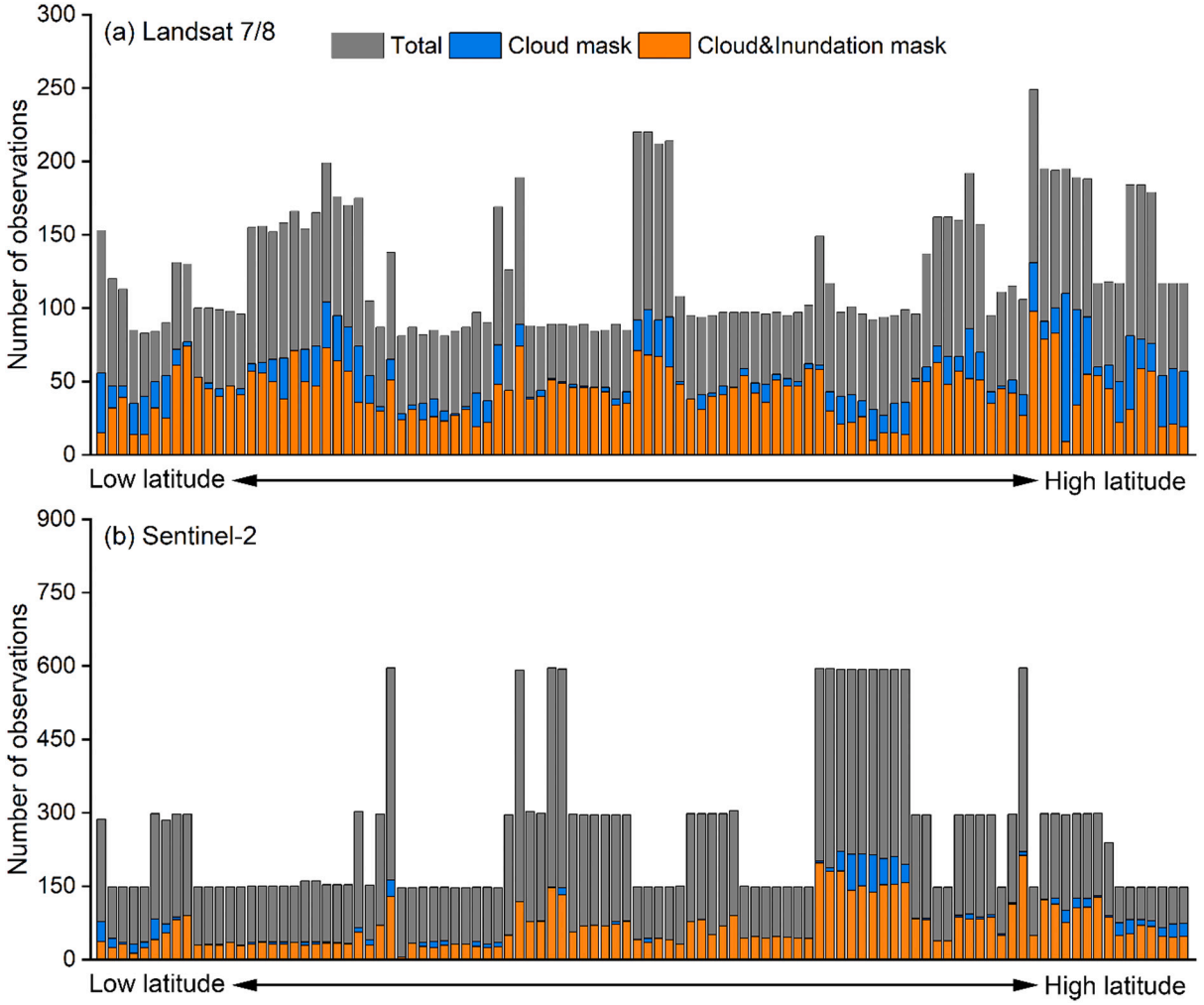

Fig. 2. The distribution of observations at selected *S. alterniflora* saltmarsh ROIs using Landsat 7/8 images (a) and Sentinel-2 images (b) during 2018–2020. The legends indicate the number of total observations, observations after cloud mask, observations after cloud and inundation mask.

often affected by tides, which may affect the surface reflectance of coastal vegetation. We excluded the observations affected by the tidal inundation for individual pixels using Eq. (4), which has been validated in previous studies (Dong et al., 2016; Xiao et al., 2006; Xiao et al., 2005). Moreover, due to the limited number of good-quality observations in coastal regions, we combined the vegetation index data from multiple years (2018–2020) into one year, organized by day of year (DOY).

$$\mathrm{NDVI} = \frac{\mathrm{NIR} - \mathrm{RED}}{\mathrm{NIR} + \mathrm{RED}} \tag{1}$$

$$\mathrm{EVI} = 2.5 \times \frac{\mathrm{NIR} - \mathrm{RED}}{\mathrm{NIR} + 6 \times \mathrm{RED} - 7.5 \times \mathrm{BLUE} + 1} \tag{2}$$

$$\mathrm{LSWI} = \frac{\mathrm{NIR} - \mathrm{SWIR}}{\mathrm{NIR} + \mathrm{SWIR}} \tag{3}$$

$$\text{Inundation observation} = \mathit{LSWI} > \mathit{NDVI} \text{ or } \mathit{LSWI} > \mathit{EVI} \tag{4}$$

where BLUE, RED, NIR, SWIR are the surface reflectance values of blue (450–515 nm), red (630–680 nm), near-infrared (NIR: 845–885 nm), and shortwave-infrared (SWIR: 1560–1660 nm) bands for OLI sensor.

Image temporal compositing is an effective approach to preprocess the time series data in many published data products (e.g., MOD13Q1), which can effectively reduce the abnormal observations due to cloud and uneven observations in time (Holben, 1986). In this study, we constructed the 10-day composites from Sentinel-2 (10-day revisit cycle) and Landsat 7/8 data by selecting the observation with the maximum value of all available observations in NDVI composites and mean value of all available observations in LSWI composites at each 10-day period. The 10-day composites start and label with 1/1, 1/11, 1/21, etc. The more specific descriptions could be found in a previous study (Liu et al., 2020a). Because the growing season of *S. alterniflora* lasts late and has some over-wintering ramets surviving until next year, we repeated the first three months (DOY 0–90) of the following year at the end of the annual time series composites to constitute a consistent annual cycle of plant growth. After obtaining the 10-day composites, we filled the missing observations using linear interpolation, and then smoothed the datasets by applying Savitzky-Golay filter with a smoothing window of size 9 and a polynomial order of 2. Because LSWI is sensitive to soil moisture (due to rainfall or inundation) and leaf water content, it is unnecessary to smooth the LSWI dataset. We did not smooth the LSWI dataset but only gap-filled the missing values. The NDVI and LSWI datasets were prepared for further phenology analysis.

2.2.2. *Field survey data*

The field surveys were conducted from August to September of 2015 across six provinces (Hebei, Shandong, Jiangsu, Zhejiang, Fujian, and Guangxi) and two municipalities (Tianjin and Shanghai) in coastal areas of China. In the field sampling work, plant and soil samples were collected and biotic and abiotic variables (e.g., aboveground biomass)

were measured. In July and September of 2020, DJI Phantom 4 Pro V2.0 Unmanned Aerial Vehicle (UAV) were also used to collect multispectral and lidar data in some coastal regions of China. The geo-referenced photos and UAV data taken from these field surveys provided information for selecting point of interest (POI). Each POI was carefully selected from saltmarsh patches larger than 60 m × 60 m to ensure the homogeneity (saltmarsh dominated) of samples. The selected POIs had consistent *S. alterniflora* saltmarshes during 2018–2020 after checking satellite images with very high spatial resolution (VHSR) from Google Earth (GE), using time slide method. Then we delineated the region of interest (ROI) as circle buffers of the points (15-m radius) using ArcGIS software. We finally generated 102 *S. alterniflora* ROIs across the coastal China to analyze the spatial variation of *S. alterniflora* saltmarsh phenology.

2.2.3. Temperature data

To analyze the temperature conditions of phenological dates (SOS, EOS) of *S. alterniflora* saltmarshes, three temperature datasets were used in this study. For air temperature (AirT), we used a climate reanalysis dataset from the European Center for Medium Range Weather Forecasts Reanalysis 5 (ECMWF/ERA5) archived in the GEE platform. ERA5 is the fifth generation ECMWF atmospheric reanalysis of the global climate and provides the available data from 1979 to three months before the real time. ERA5 dataset has a spatial resolution of 0.25 degrees. We used ERA5 daily dataset which aggregated values at each day for seven ERA5 climate reanalysis parameters including daily mean, minimum and maximum temperature at 2 m above the ground. Daily mean air temperature (T_{day}), daily daytime mean air temperature ($T_{daytime}$), and daily nighttime mean air temperature ($T_{nighttime}$) were calculated for analysis.

For sea surface temperature (SST), we used the NOAA AVHRR Pathfinder Version 5.3 (PFV53) SST dataset. These SST values were generated at approximately twice-daily 4-km resolution going back to 1981. The Pathfinder SST algorithm was applied consistently over the full time period (August 1981–December 2014) and updated till present. For land surface temperature (LST), MODIS-Aqua (MYD11A2) and MODIS-Terra (MOD11A2) products were used, which are the level-3 global Land Surface Temperature and Emissivity 8-day composites with 1-km spatial resolution. This dataset provides both daytime (LST_Day_1km) and nighttime (LST_Night_1km) surface temperatures and associated quality control assessment bands. Overpass time for daytime (nighttime) observations are about 10:30 (22:30) local solar time of Terra and about 13:30 (01,30) local solar time of Aqua. Both SST and LST datasets for the period of 2018–2020 were also processed in the GEE platform.

2.3. Phenology retrieval algorithms

Smooth cordgrass (*S. alterniflora*) is a perennial rhizomatous grass, grows 0.5–2.5 m in height, and propagates both sexually by seeds and asexually by clonal growth (Huang and Zhang, 2007). Under suitable conditions, *S. alterniflora* can reach sexual maturity after three or four months of vegetative growth. As an invasive wind-pollinated plant, *S. alterniflora* flowers from August to October, and each ramet can produce up to 800 seeds, depending on ramet size (Daehler and Strong, 1994; Qiu et al., 2018). The seed survival time is estimated to be only eight months, indicating that there is no long-term seed bank in the soil (Meng et al., 2020). According to the ground observations, *S. alterniflora* saltmarshes during winter senescence period includes (1) old dead shoots of the preceding seasons and (2) young live ramets that emerge in the fall. The new ramets generally grow about 5 cm aboveground and survive through the winter at this size and resume growth quickly in the next spring (Wijte and Gallagher, 1991).

We had time series in-situ phenology observations from an automated digital camera (Brinno BCC200) during 2018–2019 at one site on Chongming island, Shanghai. The camera has high performance HDR video sensor that generates a real time-lapse video at 5-s interval. The monthly in-situ phenological photos accompanied with air temperature, photosynthetically active radiation (PAR) from the tower site, and vegetation indices dynamics from combined Landsat/Sentinel images are shown in Fig. 3. Time series field photos show that *S. alterniflora* started to green-up in mid-April (DOY 115), grew rapidly from May to early-September, flowered in late-September, and died in late-December or January of next year (DOY 10). The site-based local weather and sensor-based greenness variation generally concur well with the observed phenology change of *S. alterniflora* saltmarshes. The phenology of plants determines the growth stage, water and chlorophyll content, and canopy structure of plants, and thus the spectral reflectance captured by portable spectrometer or satellite sensor, facilitating the derivation of phenological metrics. Table 1 shows key growth stages of *S. alterniflora* and its possible relations to the satellite-based land surface phenology.

In order to obtain robust phenology information and assess the performance of several widely used phenology retrieval methods, the phenological metrics were determined from three different retrieval algorithms in this study: NDVI-based pixel-specific statistical threshold method (hereafter, NDVI-ST), NDVI-based double logistic mathematical method (hereafter, NDVI-DLM), and LSWI-based biological threshold method (hereafter, LSWI-BT).

2.3.1. Method 1: NDVI-based pixel-specific statistical threshold method

The start of season (SOS), end of season (EOS), and length of season (LOS) were determined with a transformation of NDVI (referred as $NDVI_{ratio}$) developed by White et al. (1997). The $NDVI_{ratio}$ was calculated by the difference between the NDVI value at a certain time ($NDVI_t$) and the minimum value ($NDVI_{min}$) for the time span of interest, normalized by the amplitude of NDVI values during this time span ($NDVI_{max}$ - $NDVI_{min}$) (Eq. (5)). In the study of White et al. (1997), the threshold of 0.5 in the $NDVI_{ratio}$ curve was used to identify the onset and offset of season because it indicates the most rapid increase and decrease in greenness (greatest slope). Another study that used the ground observations at 22 grassland monitoring stations in Qinghai Province, China, reported the threshold of 0.2 for identifying the beginning of the growing season (Yu et al., 2010). In this study, we were more concerned with the date of leaf emergence, thus we used the threshold of 0.2 to determine SOS and EOS during the growth and senescence periods. The first composite with consecutive values exceeding the predefined threshold (0.2) was identified, then NDVI of two near composite periods were linearly interpolated into daily NDVI to locate the specific day of the year (DOY) as SOS. The same procedure was applied to define EOS.

$$NDVI_{ratio} = \frac{NDVI_t - NDVI_{min}}{NDVI_{max} - NDVI_{min}} \quad (5)$$

2.3.2. Method 2: NDVI-based double logistic mathematical method

A double logistic model was applied to characterize the seasonal change of *S. alterniflora* using a consistently processed 10-day NDVI composites. The double logistic model is effective for depicting plant growth curves (both green-up and senescence phases) by modeling increasing greenness in spring and decreasing greenness in autumn, which has been widely used in phenology studies (Elmore et al., 2012; Fisher et al., 2006; Zhang et al., 2003). The NDVI composites were fitted using the improved double logistic model as Eq. (6). We followed the method provided by Zhang et al. (2003) to identify phenology transition dates by calculating the rate of change in the curvature (third derivative) of the fitted logistic model. Specifically, we defined the start and end of growing season as the day when the rate of change in the curvature reached the first local maximum value and the last local minimum value, respectively. The length of growing season was calculated as the number of days between start and end of growing season.

$$f(t) = v_1 + v_2\left(\frac{1}{1+e^{-m_1(t-n_1)}} - \frac{1}{1+e^{-m_2(t-n_2)}}\right) \quad (6)$$

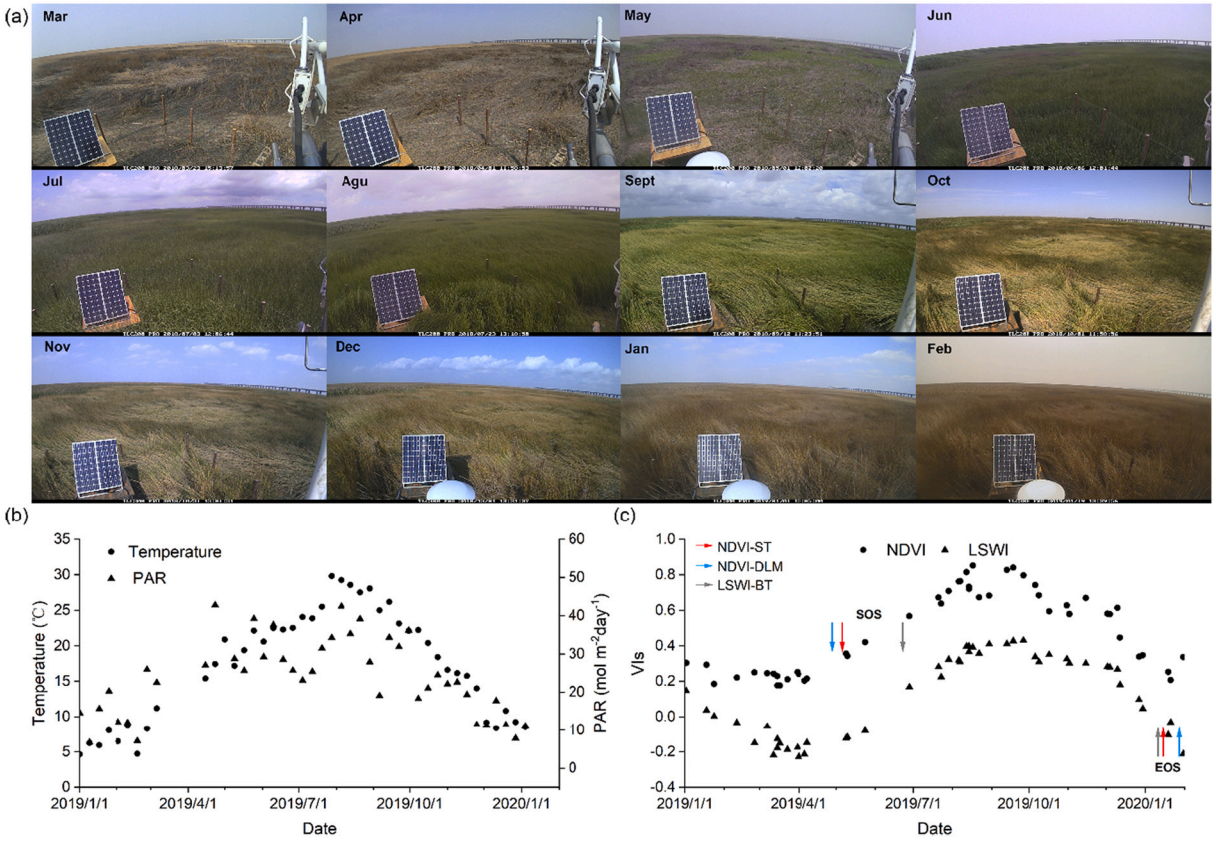

Fig. 3. Monthly phenological photographs of *Spartina alterniflora* from an in-situ site on Chongming island, Shanghai (a) and the seasonal dynamics of 8-day mean air temperature and PAR (b) and vegetation indices (c) in 2019.

Table 1
Key growth stages and descriptions of *Spartina alterniflora* and its possible relations to satellite-based land surface phenology (LSP).

Key growth stage	Description	Land surface phenology
Sprouting	Emergence of leaves from seeds and rhizomes, indicating the initial growth of plants	Greenup onset (start of the season, SOS)
Flowering	When the aboveground biomass has reached its maximum and plants switch from vegetative growth to sexual reproduction	Reaching maximum greenness
Fruiting	Seed set and maturity	Between maximum greenness and senescence onset
Senescence	Coloring of leaves and stems	Senescence onset
Dormancy	Most leaves and stems wither, a few new ramets emerge and keep green but grow very slowly, indicating the end of photosynthesis and the start of overwintering	Dormancy onset (end of the season, EOS)

where $f(t)$ is the fitted NDVI value at time t (in DOY), v_1 and v_2 are the background and amplitude of NDVI over the entire year, respectively. m_1, n_1, m_2, and n_2 are the fitted parameters that determine the slope and phase of sigmoid growth curve at both green-up and senescence phases.

2.3.3. Method 3: LSWI-based biological threshold method

The SWIR band is sensitive to both leaf water content and soil moisture, and is often used to develop water-related vegetation indices such as LSWI (Xiao et al., 2002a; Xiao et al., 2002b). Green leaves have higher NIR reflectance than SWIR reflectance, resulting in positive LSWI value (> 0). Senescent (or dead) leaves and soils have lower NIR reflectance than SWIR reflectance, resulting in negative LSWI value (< 0). For plants, the transition of LSWI <0 to LSWI >0 represents emergence of green leaves, and the transition of LSWI >0 to LSWI <0 represents a state of change from green leaves to senescent (or dead) leaves, which together are referred to as a phenology-related change in biophysical traits of leaf (Xiao et al., 2009). As coastal saltmarshes are periodically affected by tidal water, moist soils cause large spectral absorption in the SWIR band, which leads to LSWI >0. To apply this assumption to coastal saltmarshes, we slightly relaxed the specified threshold to determine the phenological transition dates: LSWI - 0.1 > 0. The adjustment of 0.1 is referred to higher soil moisture level in previous studies (Chen et al., 2018; Liu et al., 2020a). Similarly to method 1 (NDVI-ST), the first day in the spring with LSWI exceeding this threshold was defined as SOS, while the first day in the fall and winter with LSWI below this threshold was defined as EOS.

2.4. Statistical analyses

We calculated the growing degree-days (GDD), which measures the number of degrees that daily mean temperature exceeds a threshold for plant leaves to emerge or green-up, to characterize the effects of thermal conditions on spring phenology of *S. alterniflora* saltmarshes. We used 10 °C as the base temperature for *S. alterniflora*, which has been assessed by laboratory and field experiments (Kirwan et al., 2009). Accumulation of GDD (accumulated growing degree-days, AGDD) starts at the beginning of the calendar year and continues until spring green-up (SOS date). The GDD and AGDD were calculated from ERA5 AirT and MODIS LST using Eqs. (7)–(8). Note that LST dataset is 8-day composite dataset, and LST value in one 8-day period is the average value of all good-quality observations within the 8-day period. We assumed the same LST value for each day within the 8-day period, when we calculated GDD. In order to compare AGDD at SOS for different latitude bins, we drew color

scatterplots at 4-degree latitudinal interval between 20°N and 40°N. The simple linear regressions were fitted for different latitude bins and the coefficient of determination (R^2) and slopes (k) were calculated. On the other hand, in comparison to spring green-up (SOS) that needs a period of time to accumulate thermal, a few frost events are sufficient to drive leaf from green to senescence or dead, which could occur within a week or so. We calculated the 5-day mean temperature prior to EOS from the three temperature datasets to represent the temperature conditions when the fall/winter senescence (EOS) occurred. Specifically, for AirT and SST datasets, all available daily temperatures during a time period of 5 days prior to EOS were averaged; for LST 8-day composite dataset, LST from one composite prior to EOS was used. Annual mean temperature (AirT, SST, LST) and their AGDD and seasonal mean temperature (spring and winter) over five latitude bins, based on *S. alterniflora* salt-marsh ROIs, were compared (Figs. S1–S2).

$$GDD_t = \begin{cases} T_{mean,t} - T_{base} \ (T_{mean,t} > T_{base}) \\ 0 \ (T_{mean,t} \le T_{base}) \end{cases} \quad (7)$$

$$AGDD_t = \sum_{DOY=1}^{t} i \times GDD_t \quad (8)$$

where $T_{mean,t}$ is daily mean air temperature for ERA5 AirT and mean of the mean daytime ($T_{10:30}$ and $T_{13:30}$) and mean nighttime ($T_{22:30}$ and $T_{01:30}$) land surface temperature for MODIS LST at DOY (t), T_{base} is set as 10 °C, and i is the time interval coefficient (GDD from AirT is 1, GDD from LST is 8).

Prior to the phenological trend analysis, quality control of derived phenological dates was conducted to reduce uncertainties: removing those ROIs with SOS earlier than DOY 60 or later than DOY 180, and removing those ROIs with EOS later than DOY 60 of the next year. One ROI was accepted only if both SOS and EOS were available. In order to characterize the latitudinal phenology trends, we simply averaged the three phenological metrics (SOS, EOS, and LOS) within each 0.5° × 0.5° gridcell between 20°N and 40°N. Standard errors of the mean (SEM) and 95% confidence intervals were calculated to quantify the variation at each gridcell using Eq. (9). Latitudinal trends of phenology were examined by applying the least-squares linear regression model with latitude as the independent variable and phenological metrics as the response variable. Regression coefficients (R^2) and *p*-values were calculated.

$$SEM(\bar{x}) = \frac{SD}{\sqrt{n}} \quad (9)$$

where SD is the standard deviation, and n is the sample size.

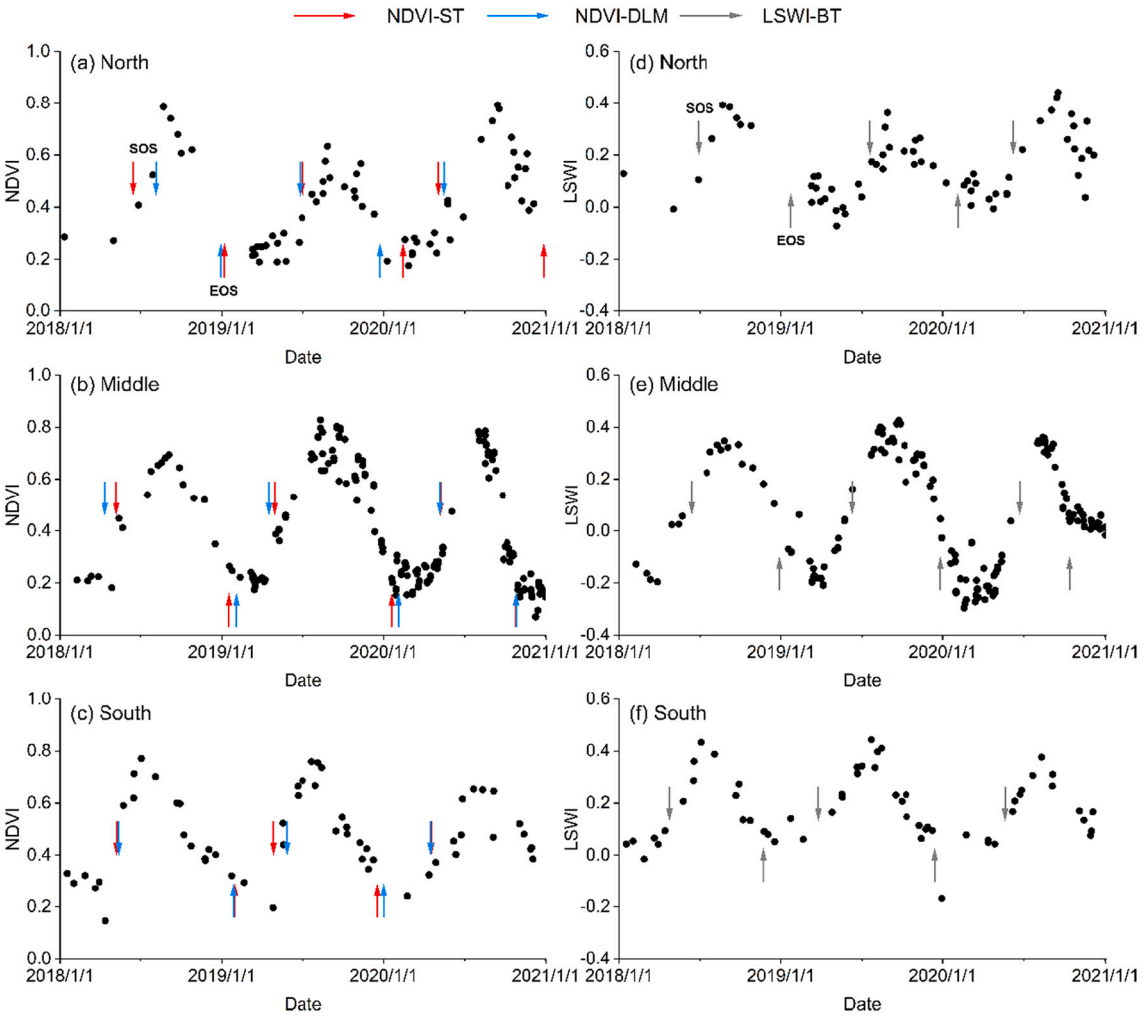

Fig. 4. Seasonal dynamics of vegetation indices (NDVI and LSWI) at three sites (North: 39.0439°N, 117.7613°E; Middle: 31.7854°N, 121.6705°E; South: 21.5872°N, 109.0414°E) from combined Landsat/Sentinel images during 2018–2020.

3. Results

3.1. Comparison of vegetation indices and phenological metrics derived from combined Landsat 7/8 and Sentinel-2 images at three sites

The seasonal and interannual dynamics of NDVI and LSWI from combined Landsat/Sentinel images at three sites (at a latitudinal interval of 10 degree) during 2018–2020 were compared (Fig. 4). NDVI and LSWI from the north, middle, and south sites had different seasonal dynamics. Greenness in spring started to rise earliest at the south site, followed by the middle and north sites. NDVI peaked around late June to July at the south site, earlier than the timing of peak at the other two sites. In the fall/winter senescence period, the rate of greenness decline at the middle site was the slowest and NDVI remained above 0.2 until January in the next year. The seasonal dynamics of LSWI was similar to that of NDVI. During winter to early spring, LSWI dropped below 0 and reached around −0.2 at the middle site, while LSWI at the north and south site decreased to around 0. SOS and EOS were calculated and marked at each year using combined Landsat/Sentinel images (Fig. 4). There were some interannual fluctuations in the estimation of phenological metrics, for example, the SOS dates were identified as 128, 116, 107 day-of-year (DOY) at the south site during the period of 2018–2020 when NDVI-ST was used.

All available observations from multiple years (2018–2020) were combined into one year to compare the phenological metrics derived from the three phenology retrieval methods and combined Landsat/Sentinel images (Table 2). It is clear that the phenological metrics retrieved from different phenology retrieval methods were slightly variable but represented similar trends among the three sites. SOS dates were earliest at the south site followed by the middle site and the north site, and EOS dates were latest at the middle site. When NDVI-DLM was used, most retrieved SOS were earlier and retrieved EOS were later than those from the other two phenology retrieval methods. Of the three sites, the middle site had the largest deviation in SOS and EOS when the three phenology retrieval methods were used.

3.2. Temperature conditions of S. alterniflora saltmarsh SOS and EOS dates

Fig. 5 shows the relationships between AGDD and SOS from 102 *S. alterniflora* saltmarsh ROIs, based on two types of temperature datasets (AirT and LST) and three phenology retrieval methods. Compared to the relationship with AGDD from AirT ($AGDD_{AirT}$), the relationship between AGDD from LST ($AGDD_{LST}$) and SOS was less obvious (Fig. 5), partially because of few available data from LST dataset. The AGDD estimates for ROIs at lower latitudes were significantly higher than those at higher latitudes, showing different optimal forcing temperature for *S. alterniflora* at different latitudes. The correlations (indicated by coefficient of determination, R^2) between AGDD and SOS across the latitudes were also different (Table 3), suggesting that temperature plays varying degrees of importance in determining the SOS dates of *S. alterniflora* saltmarshes across the latitudes. For the ROIs within the temperate zone, where temperature is a limiting factor, SOS significantly changed with AGDD. For the ROIs within the subtropical and tropical zones, where temperature is not a limiting factor, there was no significant linear relationship between AGDD and SOS. Linear regression analyses also showed that the slopes at higher latitudes were generally higher than those at lower latitudes (Table 3), which further supported the closer relationship between AGDD and SOS at higher latitudes.

Fig. 6 shows the temperature conditions of EOS from 102 *S. alterniflora* saltmarsh ROIs, based on three types of temperature datasets (AirT, SST, and LST) and three phenology retrieval methods. The temperature conditions of EOS from SST and LST datasets were far more scattered and irregular than those from AirT dataset, suggesting that AirT dataset would be more appropriate than SST and LST datasets for phenology retrieval of EOS. Among the ROIs within the temperate zone, the EOS dates at higher latitudes (≥ 36°N) were earlier, because of earlier arrival of cold temperature in the fall/winter season (Fig. 6a,b). Most of ROIs within the temperate zone started senescence when air temperature fell below 5 °C (Fig. 6a,b) and SST fell below 2 °C (Fig. 6d, e). For the ROIs within the subtropical and tropical zones, there were weak relationships between EOS and temperature, as shown by highly scattered data in Fig. 6, suggesting that temperature plays a weak role in determining the EOS dates of *S. alterniflora* saltmarshes at lower latitudes.

3.3. Latitudinal variation of S. alterniflora saltmarsh phenology across coastal China

Fig. 7 shows latitudinal variation in phenological metrics (SOS, EOS, and LOS) of *S. alterniflora* saltmarshes during 2018–2020 using three phenology retrieval methods. Despite the spatial heterogeneity, SOS became later and LOS became shorter as latitude increased across coastal China. It is clear that SOS in the north of the Yangtze River (Tianjin, Hebei, Shandong, and Jiangsu) were mostly later than DOY 120 (i.e., May or June), while SOS in the south of the Yangtze River (Shanghai, Zhejiang, Fujian, and Guangxi) mostly occurred on DOY 90–120 (i.e., April). As for EOS, no significant latitudinal trends were observed but EOS in mid-latitude regions were slightly later than those in high- and low-latitude regions. We performed quality control of the resultant phenological metrics, and then aggregated into 0.5 degree by calculating the mean value to explore the quantitative relationship between phenological metrics and latitude (Fig. 8). The relationships between phenological dates and latitudes followed similar patterns obtained by three phenology retrieval methods. The slopes of SOS, EOS, and LOS were respectively 2.54, 0.37, −2.17 from NDVI-ST, and 2.30, 0.05, −1.70 from NDVI-DLM, and 2.97, 0.99, −1.70 from LSWI-BT. The large variations in the latitudinal trend of SOS and EOS mostly occurred in the estuarine regions such as Yangtze estuary (~31°N), Oujiang estuary (~28°N), Minjiang estuary (~26°N) and Zhangjiang estuary (~24°N).

Table 2
Phenological metrics (SOS, EOS, and LOS) of three sites derived from three phenology retrieval methods with combined Landsat/Sentinel images.

Metrics	Sites	NDVI-ST	NDVI-DLM	LSWI-BT
SOS	North	138	146	169
	Middle	125	108	166
	South	107	107	120
EOS	North	357	383	383
	Middle	375	411	351
	South	351	366	346
LOS	North	219	237	214
	Middle	250	303	185
	South	244	259	266

Note: The phenological metrics are in the unit of day of year (DOY), and the derived date later than 365 means that the end of season occurs in the next year.

4. Discussion

4.1. S. alterniflora saltmarsh phenology along the latitudes in coastal China

The *S. alterniflora* saltmarshes have a large latitudinal range both in native and invaded regions (Wang et al., 2006), however, few attempts have been made to study the phenology of *S. alterniflora* saltmarshes across the latitudes. To our limited knowledge, this is the first study that evaluates latitudinal variation of *S. alterniflora* leaf phenology in the coastal zone of China using satellite data. In this study, we focused on the spring green-up (leaf-on, SOS) and fall/winter senescence (leaf-off, EOS) phenology, which is critical for assessing the effects of plant invasions on the structure and functioning of coastal saltmarshes.

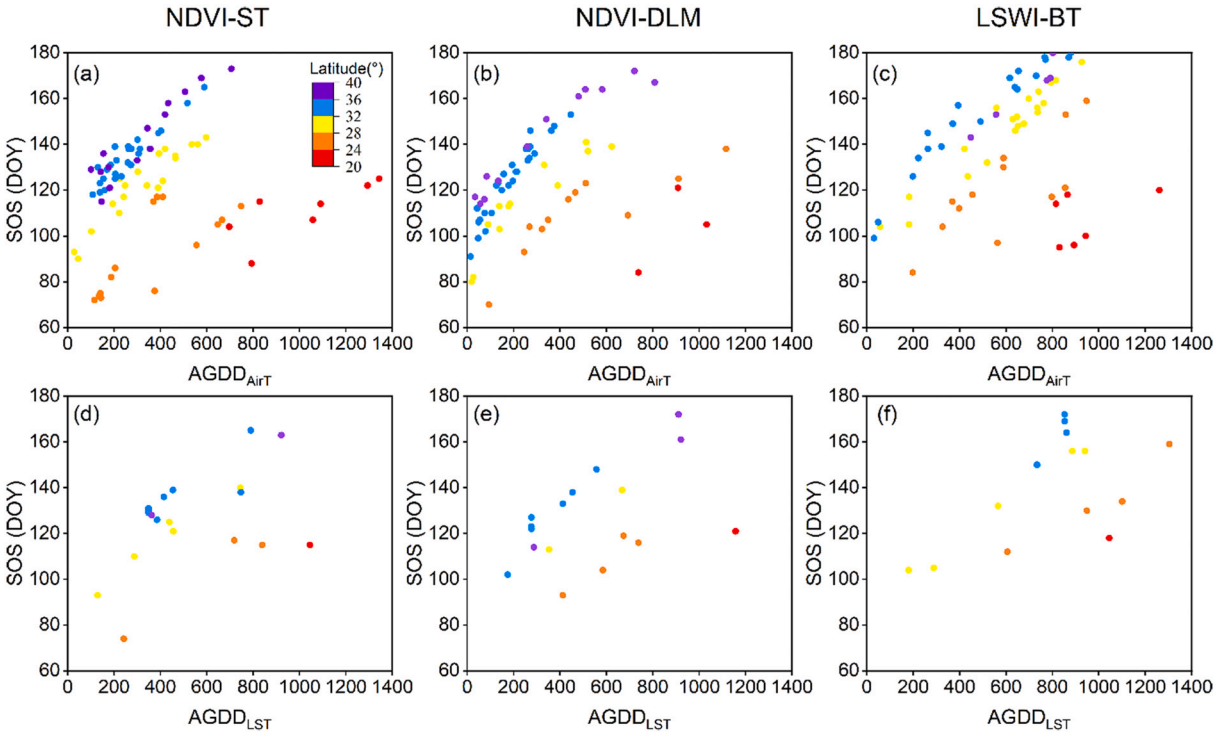

Fig. 5. The relationships between temperature conditions (AGDD) and SOS dates derived from three phenology retrieval methods and AirT (a-c) and LST (d-f) temperature datasets for 102 *S. alterniflora* saltmarsh ROIs.

Table 3
The coefficient of determination (R^2) and slopes (k) of linear regressions between $AGDD_{AirT}$ and SOS dates for different latitude bins.

Latitude bins	NDVI-ST		NDVI-DLM		LSWI-BT	
	R^2	k	R^2	k	R^2	k
20–24°N	0.58	0.0378	0.41	0.0806	0.71*	0.0476*
24–28°N	0.54*	0.0614*	0.70*	0.0499*	0.60*	0.0693*
28–32°N	0.85**	0.0852**	0.85**	0.0916**	0.93**	0.0846**
32–36°N	0.86**	0.0881**	0.91**	0.1374**	0.92**	0.0855**
36–40°N	0.88**	0.0920**	0.92**	0.0787**	0.91**	0.0952**

Note: * indicates $P < 0.01$; ** indicates $P < 0.001$.

Based on the temporal profiles of spectral bands or vegetation indices, previous studies have reported the satellite-based greenness (leaf-on or leaf-off) phenology of *S. alterniflora* saltmarshes in local regions. For instance, Sun et al. (2016), Liu et al. (2017) and Wu et al. (2020) analyzed the seasonal dynamics of vegetation indices at coastal saltmarshes from Landsat, MODIS, and Chinese Huangjing-1 (HJ-1) satellite optical imagery in Jiangsu province (~33°N), one of *S. alterniflora* invasion hotspot areas in China, and they found that *S. alterniflora* started to grow in May and died after December. Our study showed consistent but more specific results: SOS of *S. alterniflora* in Jiangsu province were mostly later than DOY 120 and EOS were mostly later than DOY 365 (January to February of the next year). Another study by Tian et al. (2020) identified the green and senescence periods of *S. alterniflora* in Beibu Gulf (18°N - 22°N) by using an average NDVI temporal profile from multi-year (2014–2017) Landsat-8 OLI images, and determined the green period from DOY 154 to 270 and the senescence period from DOY 1 to 142 of the next year. Our results for those ROIs within the latitude of 20°N - 22°N showed that SOS occurred at around DOY 110 and EOS occurred at around DOY 10 of the next year. Overall, the phenology retrievals from this study are not only in line with the findings from previous studies that covered smaller areas along the coastal China but also provide continuous phenology information that could make a quantitative analysis over a wide range of latitudes.

Our results on the latitudinal variation of EOS within the temperate zone was consistent with the Hopkins' Bioclimatic Law, which predicts that the senescence dates of plants should occur earlier as latitude increases, driven by the short photoperiod and cold temperature (Hopkins, 1920). When we did a piecewise analysis, we found that the EOS dates in mid-latitude regions were slightly later than those in low-latitude regions. Three potential causes might help explain such latitudinal pattern of EOS at *S. alterniflora* saltmarshes. First, nitrogen availability has been reported to play an important role in regulating plant growth, and the plant tended to delay the phenology when resources are abundant (e.g., nitrogen addition) (Cleland et al., 2006; Wang and Tang, 2019). Our previous study (Xu et al., 2020a) has suggested that the amount of exogenous nitrogen was highest at the mid-latitude in China and decreased with both increasing and decreasing latitude, which might have led to an later EOS at middle latitudes. Second, heat-stress which can result in an advancement of plants senescence (Xie et al., 2015) might have led to an early EOS at lower latitudes. Previous studies conducted in both native and introduced ranges suggested that at lower latitudes, extremely high temperature reduced *S. alterniflora* performance (Liu et al., 2016a; Wiski and Pennings, 2014). For example, some field-based studies found that sexual reproduction of *S. alterniflora* at lower latitudes was low as shown by minimal seed set and very small numbers of flowering culms (Liu et al., 2016a; Liu et al., 2020c). Third, the accuracy of EOS detection is affected by several factors and thus there is uncertainty in EOS estimates, which might contribute to the large scattering of EOS among the ROIs across the latitudes. Further studies are still required to investigate the mechanisms underlying the latitudinal patterns of *S. alterniflora* saltmarsh phenology.

4.2. Uncertainties in satellite-based characterization of S. alterniflora land surface phenology

Data and methods can introduce uncertainties that affect interpretations of the findings. In this study, we used time series Landsat

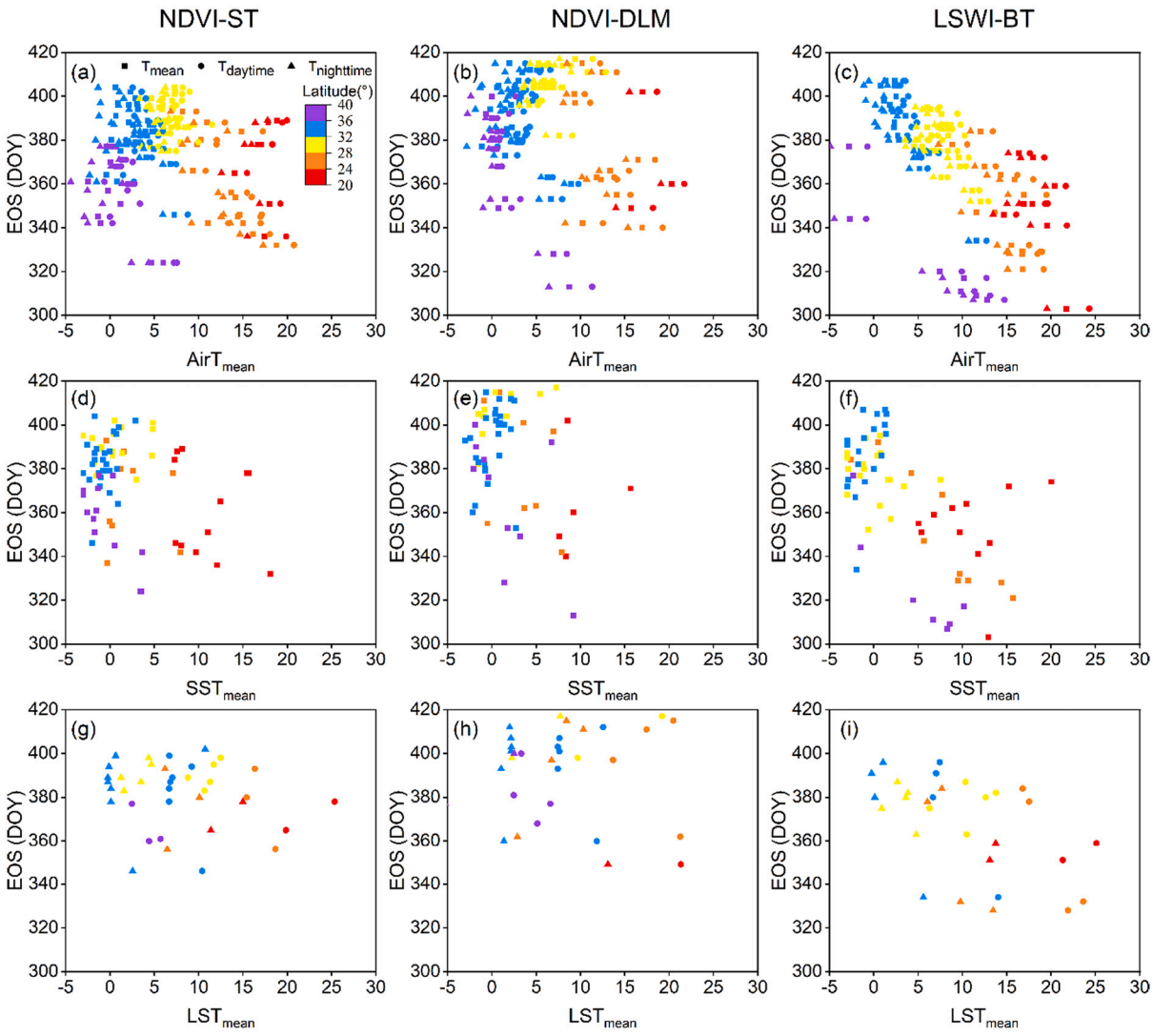

Fig. 6. The relationships between temperature conditions (mean temperature) and EOS dates derived from three phenology retrieval methods and AirT (a-c), SST (d-f), and LST (g-i) temperature datasets for 102 *S. alterniflora* saltmarsh ROIs.

7/8 and Sentinel-2 surface reflectance (SR) data to estimate land surface phenology. Due to frequent cloud coverage across the coastal zone, there were missing data after quality control (cloud and inundation mask) and the number of good-quality observations in a year at ROIs varied across the latitudes (Fig. 2), which could cause some uncertainties in the retrieval of phenological metrics. To reduce such uncertainties, we combined three-year observations into one year organized by DOY and constructed 10-day time series composites through gap-filling and data smoothing. Here we took 6 sample sites (3 pairwise adjacent sites) at different latitudes with either low or high number of observations as an example to compare the seasonal dynamics of NDVI before (raw) and after (processed) data compositing and analyzed the impact of number of observations on the retrieved phenological metrics by using NDVI-ST (Fig. 9). The data compositing process could to certain degree eliminate or reduce the impact of number of available observations on phenology retrieval.

In terms of phenology retrieval method, both NDVI-ST and NDVI-DLM are based on the seasonal variation of vegetation greenness, which is mediated by leaf chlorophyll content and canopy structure (Gitelson and Merzlyak, 1997). Previous studies on terrestrial ecosystems have noticed that, compared to spring green-up (SOS), satellite-derived vegetation senescence phenology (EOS) is more disparate with ground observations (Yan et al., 2019; Zeng et al., 2020). In contrast to the rapid leaf color change and leaf expansion during the green-up phase, the changes in leaf color and leaf area during the senescence phase are more gradual (Yan et al., 2019), limiting the ability to accurately monitor leaf senescence. As for *S. alterniflora*, the standing litter in late autumn is also likely to interfere with the decreasing NDVI trends detected from synoptic sensor. The standing litter with withered canopy dampens the reflectivity of NIR band and reduces the NDVI value. Additionally, most *S. alterniflora* populations have over-wintering ramets, and the presence of ramets in winter might also affect the satellite detection of increasing greenness in the next year. On the other hand, the LSWI-based delineation of plant growing season was first proposed in an early study of forests in Northern China (Xiao et al., 2002b), later used and developed in the study of forests in other regions (Delbart et al., 2005; Xiao et al., 2009). To date, no formal study examined the potential of LSWI-BT in extracting phenological metrics of coastal saltmarshes. In this study, we found that LSWI-BT had the lowest ability to retrieve SOS estimates (retrieval rate of 67.6%) because 1) some LSWI values did not fall below the threshold in spring onset or fall/winter offset period, and 2) excluding inundation observations reduced the data availability for temporal analysis. We therefore set quality control rules to remove the abnormal phenological retrievals before further latitudinal trend analysis.

It should be noted that there were some local variations of

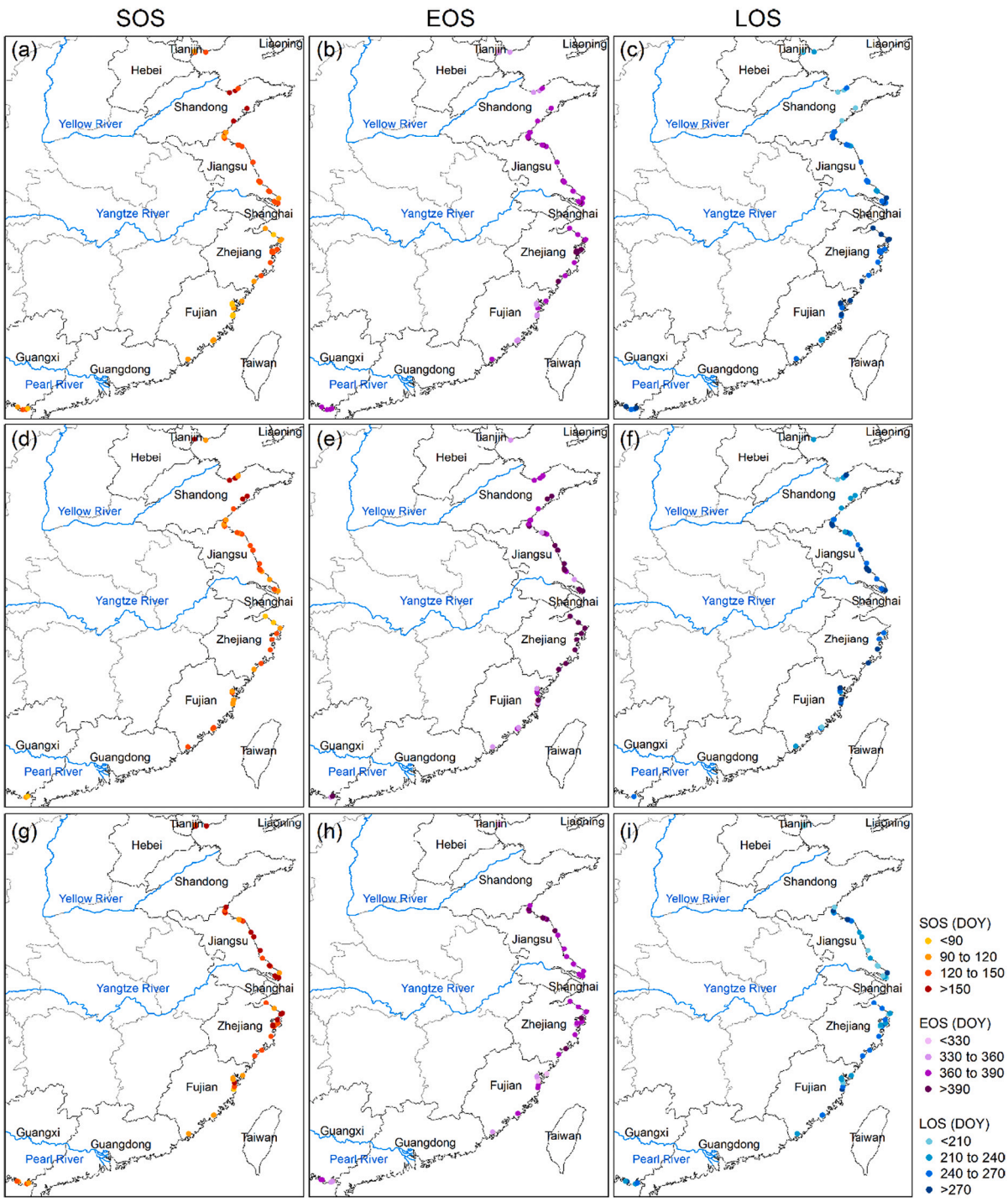

Fig. 7. Spatial variation of three phenological metrics (SOS, EOS, and LOS) of *S. alterniflora* saltmarshes at ROIs ($n = 102$) using each of the three phenology retrieval methods (NDVI-ST (a-c), NDVI-DLM (d-f), and LSWI-BT (g-i)).

phenological metrics even if the same method was adopted, which might be attributable to the selection of regions of interest (ROIs). Here, we considered two possible scenarios when the selection of ROIs affected the phenology retrievals. First, previous studies have found that the growth of invasive species may decline over time after an initial success due to the development of limiting factors (Banasiak and Meiners, 2009; Lankau et al., 2009). A field experiment with *S. alterniflora* reported that the old *S. alterniflora* populations created unsuitable habitats for themselves by reducing the tidal inundation time and changing the available resources of light and space (Tang et al., 2012). Therefore, the selected ROIs with different population ages (i.e., invasion age) could cause the local variation of extracted phenological dates. Second, the selected ROIs distributed in different tidal heights (or distance from the sea) also cause the variation of extracted phenological dates over short distances in the natural environment. By analyzing 294 Landsat 5 TM scenes acquired between 1984 and 2011, O'Donnell and Schalles (2016) found that tall form *S. alterniflora* standing at lower elevations and more favorable edaphic conditions had earlier and more robust spring growth. Another study found that spring green-up of plants in the interior area was 17 days earlier than that of plants at the channel edges, and they attributed this phenomenon to the elevation changes (15 cm) that drove soil temperature variation of 0.8 °C (O'Connell et al., 2019). In addition,

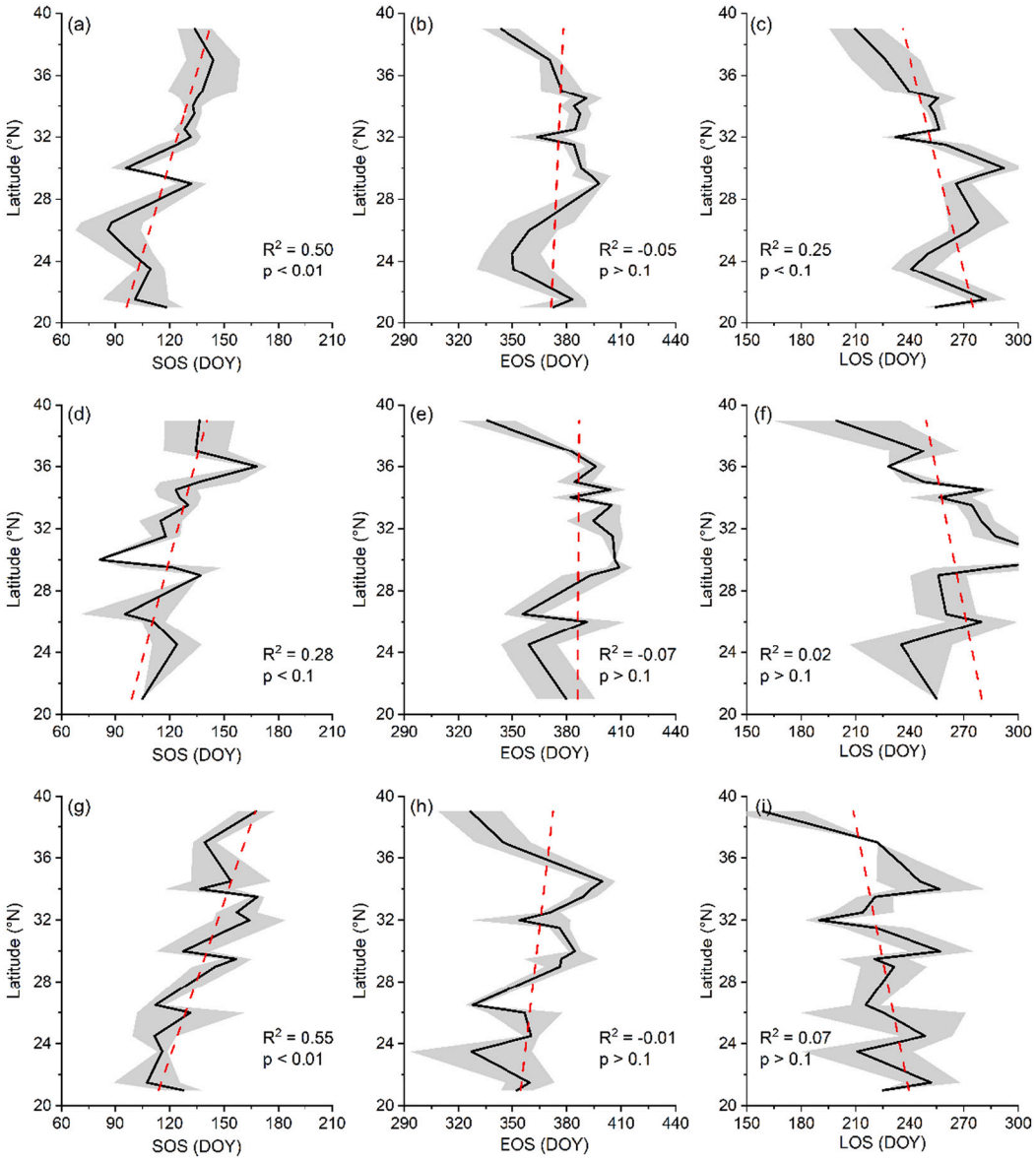

Fig. 8. The mean phenological metrics along the latitude at 0.5° spatial resolution, derived from NDVI-ST (a-c), NDVI-DLM (d-f), and LSWI-BT (g-i). The red dashed lines show the linear trend of relationship and the shaded areas represent standard errors of the mean. (For interpretation of the references to color in this figure legend, the reader is referred to the web version of this article.)

a recent study developing *S. alterniflora* mapping algorithm also found that the spatial variation of phenology existed in *S. alterniflora* (Tian et al., 2020). Therefore, in this study, we aggregated the SOS, EOS, and LOS for each 0.5° × 0.5° gridcell, which could reduce the local variations in characterizing the overall latitudinal trend of *S. alterniflora* saltmarsh phenology.

4.3. Implications for coastal ecosystem management

Our study provided a quantitative comparison of SOS, EOS, and LOS of *S. alterniflora* saltmarshes along the latitudinal gradient in the coastal zone of China. The latitudinal phenology information obtained from this study is expected to significantly improve the *S. alterniflora* saltmarsh mapping as the phenology-based algorithm is quite prevalent in land cover classification recently (Dong et al., 2016; Helman et al., 2015). Due to the phenological variation of *S. alterniflora* along a geographic gradient, previous studies using the phenology-based mapping tool only identified and generated the distribution of *S. alterniflora* saltmarshes at certain locations (Ai et al., 2017; Sun et al., 2016; Tian et al., 2020; Zhang et al., 2020). With the comprehensive phenology information across the latitude, researchers could now adjust their algorithms, for example, determining the optimal temporal windows, and apply it to map the *S. alterniflora* saltmarshes over large geographic regions. If so, the resultant *S. alterniflora* saltmarsh maps across coastal China would provide useful knowledge for the management of this invasive species and coastal ecosystem.

Latitudinal phenology information can also help understand the effects of *S. alterniflora* invasion on structure and functioning (e.g., productivity) of coastal wetlands. The timing of green-up and senescence determines the length of growing season, which is proportional to the CO_2 uptake period (CUP) and indicates the duration of CO_2 assimilation within a year. It has been acknowledged that the terrestrial gross primary production is jointly controlled by vegetation phenology and physiological processes (Xia et al., 2015). For coastal ecosystems, with the latitudinal phenology information of *S. alterniflora* saltmarshes, we are able to estimate the total carbon (blue carbon) sequestrated by

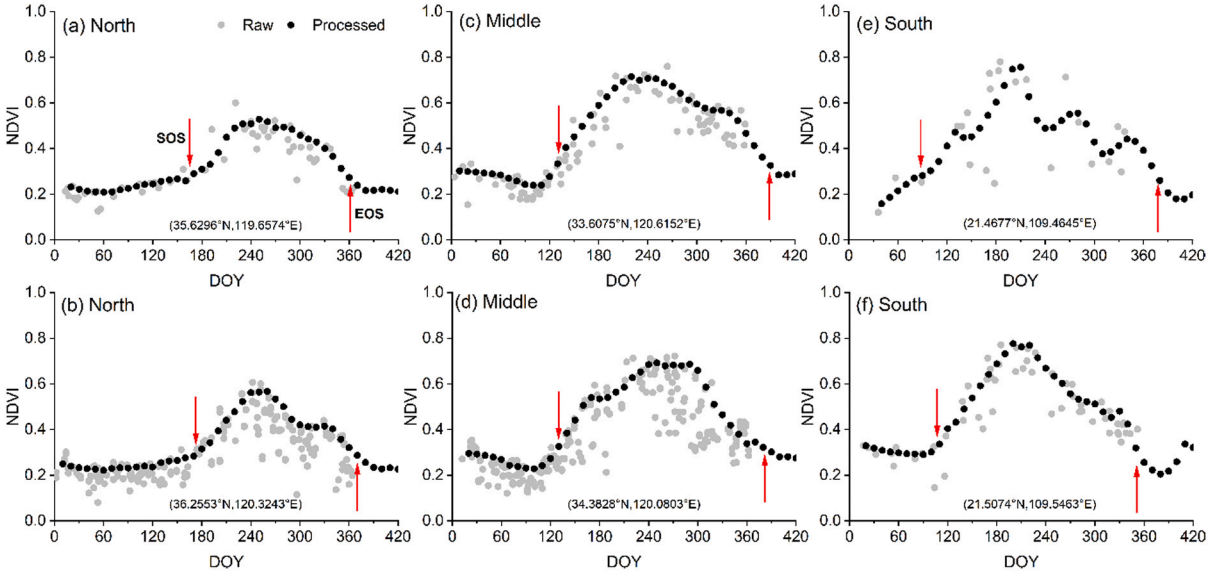

Fig. 9. The seasonal dynamics of raw and processed NDVI data at 6 sample sites (3 pairwise) with low (a, c, e) and high (b, d, f) number of observations in high-latitude (north), middle-latitude (middle), and low-latitude (south) regions.

S. alterniflora saltmarshes across the latitudes. Some previous studies have suggested that the rapid expansion of *S. alterniflora* would make it the leading contributor to primary production in the coastal marshes especially because they have higher photosynthesis efficiency, higher LAI, and longer growing season (Ge et al., 2016; Ge et al., 2015; Liao et al., 2007). The comprehensive latitudinal phenology knowledge of *S. alterniflora* saltmarshes provides valuable and timely information for different decision makers and stakeholders to efficiently manage the saltmarshes and coastal wetlands in general.

In addition, a number of studies have pointed out that the capability of invasion for an exotic species depends largely on its phenological characteristics (Fridley, 2012; Wolkovich and Cleland, 2014). Under ongoing global warming, if we extend the phenology information to both temporal and spatial scales, we are able to predict the new invasions based on their phenological sensitivity and latitudinal phenology patterns, which support to establish an early-warning system against plant invasions.

5. Conclusions

This study demonstrates the capacity of time series Landsat 7/8 and Sentinel-2 images to identify and characterize phenology of *S. alterniflora* saltmarshes over 102 sites along the latitudinal gradient in coastal China. After combining Landsat 7/8 and Sentinel-2 images, more good-quality observations were used to track the seasonal dynamics of *S. alterniflora* saltmarshes, which conduces to generate more reasonable phenological retrievals. These three phenology retrieval methods generated reasonable phenological metrics (SOS and EOS dates). The temperature conditions over the time periods associated with those SOS and EOS dates meet the biological temperature requirements for vegetation green-up or senescence. The SOS dates of *S. alterniflora* saltmarshes varied across the latitudes with a significant linear trend, and there is a linear relationship between AGDD and SOS for those ROIs in the temperate zone. The EOS dates of *S. alterniflora* saltmarshes varied across the latitudes without a linear trend. Because the relationship between SOS and the latitudes was significantly positive, the relationship between LOS and the latitudes was significantly negative. As more ground phenology monitoring sites for *S. alterniflora* saltmarshes become available in the future, the satellite-based phenology could be validated and integrated with ground observations to accurately and dynamically monitor the large-scale phenology change of *S. alterniflora* saltmarshes and other invasive plants, which could support the management of invasive species and coastal wetland ecosystems.

Declaration of Competing Interest

The authors declare that they have no known competing financial interests or personal relationships that could have appeared to influence the work reported in this paper.

Acknowledgements

The study was supported by the National Natural Science Foundation of China, China (41630528, 32030067, 41371258, and 81961128002), U.S. National Science Foundation (1911955), and China Postdoctoral Science Foundation (2021TQ0072). We sincerely thank Lianghao Pan, Dr. Youzheng Zhang, and Dr. Jun Ma for providing the geo-referenced field photos and UAV data. We appreciate Dr. Haiqiang Guo and Songshuo Li for providing in-situ phenological observations and meteorological data from flux tower site on Chongming island, Shanghai. We thank the reviewers for their constructive comments that helped us to revise this manuscript.

Appendix A. Supplementary data

Supplementary data to this article can be found online at https://doi.org/10.1016/j.rse.2021.112810.

References

Ai, J., Gao, W., Gao, Z., Shi, R., Zhang, C., 2017. Phenology-based Spartina alterniflora mapping in coastal wetland of the Yangtze Estuary using time series of GaoFen satellite no. 1 wide field of view imagery. J. Appl. Remote Sens. 11, 026020.

Banasiak, S.E., Meiners, S.J., 2009. Long term dynamics of Rosa multiflora in a successional system. Biol. Invasions 11, 215–224.

Bolton, D.K., Friedl, M.A., 2013. Forecasting crop yield using remotely sensed vegetation indices and crop phenology metrics. Agric. For. Meteorol. 173, 74–84.

Bórnez, K., Descals, A., Verger, A., Peñuelas, J., 2020. Land surface phenology from VEGETATION and PROBA-V data. Assessment over deciduous forests. Int. J. Appl. Earth Obs. 84, 101974.

Chen, B., Xiao, X., Ye, H., Ma, J., Doughty, R., Li, X., Zhao, B., Wu, Z., Sun, R., Dong, J., Qin, Y., Xie, G., 2018. Mapping Forest and their spatial-temporal changes from 2007 to 2015 in tropical Hainan Island by integrating ALOS/ALOS-2 L-band SAR and Landsat optical images. IEEE J. Sel. Top. Appl. Earth Observ. Remote Sens. 11, 852–867.

Cleland, E.E., Chiariello, N.R., Loarie, S.R., Mononey, H.A., Field, C.B., 2006. Diverse responses of phenology to global changes in a grassland ecosystem. Proc. Natl. Acad. Sci. U. S. A. 103, 13740–13744.
Daehler, C.C., Strong, D.R., 1994. Variable reproductive output among clones of *Spartina alterniflora* (Poaceae) invading San Francisco Bay, California: the influence of herbivory, pollination, and establishment site. Am. J. Bot. 81.
Dawson, W., Moser, D., van Kleunen, M., Kreft, H., Pergl, J., Pysek, P., Weigelt, P., Winter, M., Lenzner, B., Blackburn, T.M., Dyer, E.E., Cassey, P., Scrivens, S.L., Economo, E.P., Guenard, B., Capinha, C., Seebens, H., Garcia-Diaz, P., Nentwig, W., Garcia-Berthou, E., Casal, C., Mandrak, N.E., Fuller, P., Meyer, C., Essl, F., 2017. Global hotspots and correlates of alien species richness across taxonomic groups. Nat. Ecol. Evol. 1, 0186.
de Beurs, K.M., Henebry, G.M., 2004. Land surface phenology, climatic variation, and institutional change: analyzing agricultural land cover change in Kazakhstan. Remote Sens. Environ. 89, 497–509.
de Beurs, K.M., Henebry, G.M., 2005. Land surface phenology and temperature variation in the international geosphere-biosphere program high-latitude transects. Glob. Chang. Biol. 11, 779–790.
Delbart, N., Kergoat, L., Le Toan, T., Lhermitte, J., Picard, G., 2005. Determination of phenological dates in boreal regions using normalized difference water index. Remote Sens. Environ. 97, 26–38.
Dong, J., Xiao, X., Kou, W., Qin, Y., Zhang, G., Li, L., Jin, C., Zhou, Y., Wang, J., Biradar, C., Liu, J., Moore, B., 2015. Tracking the dynamics of paddy rice planting area in 1986-2010 through time series Landsat images and phenology-based algorithms. Remote Sens. Environ. 160, 99–113.
Dong, J., Xiao, X., Menarguez, M.A., Zhang, G., Qin, Y., Thau, D., Biradar, C., Moore, B., 2016. Mapping paddy rice planting area in northeastern Asia with Landsat 8 images, phenology-based algorithm and Google Earth Engine. Remote Sens. Environ. 185, 142–154.
Egan, T.P., Ungar, I.A., 1999. The effects of temperature and seasonal change on the germination of two salt marsh species, Atriplex prostrata and Salicornia europaea, along a salinity gradient. Int. J. Plant Sci. 160, 861–867.
Elmore, A.J., Guinn, S.M., Minsley, B.J., Richardson, A.D., 2012. Landscape controls on the timing of spring, autumn, and growing season length in mid-Atlantic forests. Glob. Chang. Biol. 18, 656–674.
Esch, E.H., Lipson, D.A., Cleland, E.E., 2019. Invasion and drought alter phenological sensitivity and synergistically lower ecosystem production. Ecology 100, e02802.
Fisher, J.I., Mustard, J.F., 2007. Cross-scalar satellite phenology from ground, Landsat, and MODIS data. Remote Sens. Environ. 109, 261–273.
Fisher, J., Mustard, J., Vadeboncoeur, M., 2006. Green leaf phenology at Landsat resolution: scaling from the field to the satellite. Remote Sens. Environ. 100, 265–279.
Fridley, J.D., 2012. Extended leaf phenology and the autumn niche in deciduous forest invasions. Nature 485, 359–362.
Garrity, S.R., Bohrer, G., Maurer, K.D., Mueller, K.L., Vogel, C.S., Curtis, P.S., 2011. A comparison of multiple phenology data sources for estimating seasonal transitions in deciduous forest carbon exchange. Agric. For. Meteorol. 151, 1741–1752.
Ge, Z., Guo, H., Zhao, B., Zhang, L., 2015. Plant invasion impacts on the gross and net primary production of the salt marsh on eastern coast of China: insights from leaf to ecosystem. J. Geophys. Res. Biogeosci. 120, 169–186.
Ge, Z., Guo, H., Zhao, B., Zhang, C., Peltola, H., Zhang, L., 2016. Spatiotemporal patterns of the gross primary production in the salt marshes with rapid community change: a coupled modeling approach. Ecol. Model. 321, 110–120.
Ghosh, S., Mishra, D., 2017. Analyzing the long-term phenological trends of salt marsh ecosystem across coastal LOUISIANA. Remote Sens. 9, 1340.
Gitelson, A.A., Merzlyak, M.N., 1997. Remote estimation of chlorophyll content in higher plant leaves. Int. J. Remote Sens. 18, 2691–2697.
Han, G., Xu, J., 2013. Land surface phenology and land surface temperature changes along an urban-rural gradient in Yangtze River Delta, China. Environ. Manag. 52, 234–249.
Hassan, Q.K., Rahman, K.M., 2012. Applicability of remote sensing-based surface temperature regimes in determining deciduous phenology over boreal forest. J. Plant Ecol. 6, 84–91.
Helman, D., Lensky, I., Tessler, N., Osem, Y., 2015. A phenology-based method for monitoring woody and herbaceous vegetation in Mediterranean forests from NDVI time series. Remote Sens. 7, 12314–12335.
Holben, B.N., 1986. Characteristics of maximum-value composite images from temporal AVHRR data. Int. J. Remote Sens. 7, 1417–1434.
Hopkins, A.D., 1920. The bioclimatic law. J. Wash. Acad. Sci. 10, 34–40.
Huang, H., Zhang, L., 2007. A study of the population dynamics of Spartina alterniflora at Jiuduansha shoals, Shanghai, China. Ecol. Eng. 29, 164–172.
Huang, Liu, Zhu, Atzberger, Liu, 2019. The optimal threshold and vegetation index time series for retrieving crop phenology based on a modified dynamic threshold method. Remote Sens. 11, 2725.
Kirwan, M.L., Guntenspergen, G.R., Morris, J.T., 2009. Latitudinal trends in Spartina alterniflora productivity and the response of coastal marshes to global change. Glob. Chang. Biol. 15, 1982–1989.
Krehbiel, C., Zhang, X., Henebry, G., 2017. Impacts of thermal time on land surface phenology in urban areas. Remote Sens. 9, 499.
Lankau, R.A., Nuzzo, V., Spyreas, G., Davis, A.S., 2009. Evolutionary limits ameliorate the negative impact of an invasive plant. Proc. Natl. Acad. Sci. U. S. A. 106, 15362–15367.
Liao, C., Luo, Y., Jiang, L., Zhou, X., Wu, X., Fang, C., Chen, J., Li, B., 2007. Invasion of Spartina alterniflora enhanced ecosystem carbon and nitrogen stocks in the Yangtze Estuary, China. Ecosystems 10, 1351–1361.
Liu, W., Maung-Douglass, K., Strong, D.R., Pennings, S.C., Zhang, Y., Mack, R., 2016a. Geographical variation in vegetative growth and sexual reproduction of the invasive Spartina alterniflora in China. J. Ecol. 104, 173–181.
Liu, Y., Wu, C., Peng, D., Xu, S., Gonsamo, A., Jassal, R.S., Altaf Arain, M., Lu, L., Fang, B., Chen, J.M., 2016b. Improved modeling of land surface phenology using MODIS land surface reflectance and temperature at evergreen needleleaf forests of Central North America. Remote Sens. Environ. 176, 152–162.
Liu, X., Liu, H., Gong, H., Lin, Z., Lv, S., 2017. Appling the one-class classification method of Maxent to detect an invasive plant Spartina alterniflora with time-series analysis. Remote Sens. 9, 1120.
Liu, L., Xiao, X., Qin, Y., Wang, J., Xu, X., Hu, Y., Qiao, Z., 2020a. Mapping cropping intensity in China using time series Landsat and Sentinel-2 images and Google Earth Engine. Remote Sens. Environ. 239, 111624.
Liu, W., Chen, X., Strong, D.R., Pennings, S.C., Kirwan, M.L., Chen, X., Zhang, Y., 2020b. Climate and geographic adaptation drive latitudinal clines in biomass of a widespread saltmarsh plant in its native and introduced ranges. Limnol. Oceanogr. 65, 1399–1409.
Liu, W., Zhang, Y., Chen, X., Maung-Douglass, K., Strong, D.R., Pennings, S.C., 2020c. Contrasting plant adaptation strategies to latitude in the native and invasive range of Spartina alterniflora. New Phytol. 226, 623–634.
Mark, V.K., Oliver, B., Wayne, D., 2018. The ecology and evolution of alien plants. Annu. Rev. Ecol. Ecol. Syst. 49, 25–47.
Melaas, E.K., Friedl, M.A., Zhu, Z., 2013. Detecting interannual variation in deciduous broadleaf forest phenology using Landsat TM/ETM+ data. Remote Sens. Environ. 132, 176–185.
Meng, W., Feagin, R.A., Innocenti, R.A., Hu, B., He, M., Li, H., 2020. Invasion and ecological effects of exotic smooth cordgrass Spartina alterniflora in China. Ecol. Eng. 143, 105670.
Nguyen, L.H., Joshi, D.R., Clay, D.E., Henebry, G.M., 2020. Characterizing land cover/land use from multiple years of Landsat and MODIS time series: a novel approach using land surface phenology modeling and random forest classifier. Remote Sens. Environ. 238, 111017.
O'Connell, J.L., Alber, M., Pennings, S.C., 2019. Microspatial differences in soil temperature cause phenology change on par with long-term climate warming in salt marshes. Ecosystems 23, 498–510.
O'Donnell, J.P.R., Schalles, J.F., 2016. Examination of abiotic drivers and their influence on Spartina alterniflora biomass over a twenty-eight year period using Landsat 5 TM satellite imagery of the Central Georgia coast. Remote Sens. 8, 477.
Palmer, S.C.J., Odermatt, D., Hunter, P.D., Brockmann, C., Présing, M., Balzter, H., Tóth, V.R., 2015. Satellite remote sensing of phytoplankton phenology in Lake Balaton using 10years of MERIS observations. Remote Sens. Environ. 158, 441–452.
Piao, S., Liu, Q., Chen, A., Janssens, I.A., Fu, Y., Dai, J., Liu, L., Lian, X., Shen, M., Zhu, X., 2019. Plant phenology and global climate change: current progresses and challenges. Glob. Chang. Biol. 25, 1922–1940.
Qiu, S., Xu, X., Liu, S., Liu, W., Liu, J., Nie, M., Shi, F., Zhang, Y., Weiner, J., Li, B., 2018. Latitudinal pattern of flowering synchrony in an invasive wind-pollinated plant. Proc. R. Soc. B-Biol. Sci. 285, 8.
R Core Team, 2013. R: A Language and Environment for Statistical Computing. R Fundation for Statistical Computing, Vienna, Austria.
Reed, B., Schwartz, M., Xiao, X., 2009. Remote sensing phenology: Status and the way forward. In: Noormets, Asko (Ed.), Phenology of Ecosystem Processes: Applications in Global Change Research. Springer, New York, pp. 231–246.
Roy, D.P., Kovalskyy, V., Zhang, H.K., Vermote, E.F., Yan, L., Kumar, S.S., Egorov, A., 2016. Characterization of Landsat-7 to Landsat-8 reflective wavelength and normalized difference vegetation index continuity. Remote Sens. Environ. 185, 57–70.
Schwartz, M.D., Reed, B.C., 1999. Surface phenology and satellite sensor-derived onset of greenness: An initial comparison. Int. J. Remote Sens. 20, 3451–3457.
Shang, L., Qiu, S., Huang, J., Li, B., 2015. Invasion of Spartina alterniflora in China is greatly facilitated by increased growth and clonality: a comparative study of native and introduced populations. Biol. Invasions 17, 1327–1339.
Shen, M., Tang, Y., Chen, J., Zhu, X., Zheng, Y., 2011. Influences of temperature and precipitation before the growing season on spring phenology in grasslands of the central and eastern Qinghai-Tibetan Plateau. Agric. For. Meteorol. 151, 1711–1722.
Shen, M., Piao, S., Chen, X., An, S., Fu, Y.H., Wang, S., Cong, N., Janssens, I.A., 2016. Strong impacts of daily minimum temperature on the green-up date and summer greenness of the Tibetan Plateau. Glob. Chang. Biol. 22, 3057–3066.
Sun, C., Liu, Y., Zhao, S., Zhou, M., Yang, Y., Li, F., 2016. Classification mapping and species identification of salt marshes based on a short-time interval NDVI time-series from HJ-1 optical imagery. Int. J. Appl. Earth Obs. 45, 27–41.
Tang, L., Gao, Y., Wang, C.-H., Zhao, B., Li, B., 2012. A plant invader declines through its modification to habitats: a case study of a 16-year chronosequence of Spartina alterniflora invasion in a salt marsh. Ecol. Eng. 49, 181–185.
Tian, J., Wang, L., Yin, D., Li, X., Diao, C., Gong, H., Shi, C., Menenti, M., Ge, Y., Nie, S., Ou, Y., Song, X., Liu, X., 2020. Development of spectral-phenological features for deep learning to understand Spartina alterniflora invasion. Remote Sens. Environ. 242, 111745.
Turbelin, A.J., Malamud, B.D., Francis, R.A., 2017. Mapping the global state of invasive alien species: patterns of invasion and policy responses. Glob. Ecol. Biogeogr. 26, 78–92.
Wang, C., Tang, Y., 2019. Responses of plant phenology to nitrogen addition: a meta-analysis. Oikos 128, 1243–1253.
Wang, Q., An, S.Q., Ma, Z.J., Zhao, B., Bo, L., 2006. Invasive Spartina alterniflora: biology, ecology and management. Acta Phytotaxon. Sin. 44, 559–588 (in Chinese).

White, M.A., Thornton, P.E., Running, S.W., 1997. A continental phenology model for monitoring vegetation responses to interannual climatic variability. Global Biogeochem. Cy 11, 217–234.
White, M.A., de Beurs, K.M., Didan, K., Inouye, D.W., Richardson, A.D., Jensen, O.P., O'Keefe, J., Zhang, G., Nemani, R.R., van Leeuwen, W.J.D., Brown, J.F., de Wit, A., Schaepman, M., Lin, X., Dettinger, M., Bailey, A.S., Kimball, J., Schwartz, M.D., Baldocchi, D.D., Lee, J.T., Lauenroth, W.K., 2009. Intercomparison, interpretation, and assessment of spring phenology in North America estimated from remote sensing for 1982-2006. Glob. Chang. Biol. 15, 2335–2359.
Wieski, K., Pennings, S., 2014. Climate drivers of *Spartina alterniflora* Saltmarsh production in Georgia, USA. Ecosystems 17, 473–484.
Wijte, A.H., Gallagher, J.L., 1991. The importance of dead and young live shoots of Spartina alterniflora (Poaceae) in a mid-latitude salt marsh for overwintering and recoverability of underground reserves. Bot. Gaz. 152, 509–513.
Willis, C.G., Ruhfel, B.R., Primack, R.B., Miller-Rushing, A.J., Losos, J.B., Davis, C.C., 2010. Favorable climate change response explains non-native species' success in Thoreau's woods. PLoS One 5, e8878.
Wiski, K., Pennings, S.C., 2014. Climate drivers of Spartina alterniflora saltmarsh production in Georgia, USA. Ecosystems 17, 473–484.
Wolkovich, E.M., Cleland, E.E., 2011. The phenology of plant invasions: a community ecology perspective. Front. Ecol. Environ. 9, 287–294.
Wolkovich, E.M., Cleland, E.E., 2014. Phenological niches and the future of invaded ecosystems with climate change. AoB Plants 6, 490–552.
Wu, Y., Xiao, X., Chen, B., Ma, J., Wang, X., Zhang, Y., Zhao, B., Li, B., 2020. Tracking the phenology and expansion of Spartina alterniflora coastal wetland by time series MODIS and Landsat images. Multimed. Tools Appl. 79, 5175–5195.
Xia, J., Niu, S., Ciais, P., Janssens, I.A., Chen, J., Ammann, C., Arain, A., Blanken, P.D., Cescatti, A., Bonal, D., Buchmann, N., Curtis, P.S., Chen, S., Dong, J., Flanagan, L.B., Frankenberg, C., Georgiadis, T., Gough, C.M., Hui, D., Kiely, G., Li, J., Lund, M., Magliulo, V., Marcolla, B., Merbold, L., Montagnani, L., Moors, E.J., Olesen, J.E., Piao, S., Raschi, A., Roupsard, O., Suyker, A.E., Urbaniak, M., Vaccari, F.P., Varlagin, A., Vesala, T., Wilkinson, M., Weng, E., Wohlfahrt, G., Yan, L., Luo, Y., 2015. Joint control of terrestrial gross primary productivity by plant phenology and physiology. Proc. Natl. Acad. Sci. U. S. A. 112, 2788–2793.
Xiao, X., Boles, S., Frolking, S., Salas, W., Moore, B., Li, C., He, L., Zhao, R., 2002a. Observation of flooding and rice transplanting of paddy rice fields at the site to landscape scales in China using VEGETATION sensor data. Int. J. Remote Sens. 23, 3009–3022.
Xiao, X., Boles, S., Liu, J., Zhuang, D., Liu, M., 2002b. Characterization of forest types in Northeastern China, using multi-temporal SPOT-4 VEGETATION sensor data. Remote Sens. Environ. 82, 335–348.
Xiao, X., Boles, S., Liu, J., Zhuang, D., Frolking, S., Li, C., Salas, W., Moore, B., 2005. Mapping paddy rice agriculture in southern China using multi-temporal MODIS images. Remote Sens. Environ. 95, 480–492.
Xiao, X., Boles, S., Frolking, S., Li, C., Babu, J.Y., Salas, W., Moore, B., 2006. Mapping paddy rice agriculture in South and Southeast Asia using multi-temporal MODIS images. Remote Sens. Environ. 100, 95–113.
Xiao, X., Biradar, C., Czarnecki, C., Alabi, T., Keller, M., 2009. A simple algorithm for large-scale mapping of evergreen forests in Tropical America, Africa and Asia. Remote Sens. 1, 355–374.
Xie, Y., Wang, X., Silander Jr., J.A., 2015. Deciduous forest responses to temperature, precipitation, and drought imply complex climate change impacts. Proc. Natl. Acad. Sci. U. S. A. 112, 13585–13590.
Xu, X., Liu, H., Liu, Y., Zhou, C., Pan, L., Fang, C., Nie, M., Li, B., 2020a. Human eutrophication drives biogeographic salt marsh productivity patterns in China. Ecol. Appl. 30, e02045.
Xu, X., Zhou, G., Du, H., Mao, F., Xu, L., Li, X., Liu, L., 2020b. Combined MODIS land surface temperature and greenness data for modeling vegetation phenology, physiology, and gross primary production in terrestrial ecosystems. Sci. Total Environ. 726, 137948.
Yan, D., Scott, R.L., Moore, D.J.P., Biederman, J.A., Smith, W.K., 2019. Understanding the relationship between vegetation greenness and productivity across dryland ecosystems through the integration of PhenoCam, satellite, and eddy covariance data. Remote Sens. Environ. 223, 50–62.
Yu, H., Luedeling, E., Xu, J., 2010. Winter and spring warming result in delayed spring phenology on the Tibetan Plateau. Proc. Natl. Acad. Sci. U. S. A. 107, 22151–22156.
Zeng, L., Wardlow, B.D., Xiang, D., Hu, S., Li, D., 2020. A review of vegetation phenological metrics extraction using time-series, multispectral satellite data. Remote Sens. Environ. 237, 111511.
Zettlemoyer, M.A., Schultheis, E.H., Lau, J.A., 2019. Phenology in a warming world: differences between native and non-native plant species. Ecol. Lett. 22, 1253–1263.
Zhang, X., Friedl, M.A., Schaaf, C.B., Strahler, A.H., Hodges, J.C.F., Gao, F., Reed, B.C., Huete, A., 2003. Monitoring vegetation phenology using MODIS. Remote Sens. Environ. 84, 471–475.
Zhang, X., Friedl, M.A., Schaaf, C.B., Strahler, A.H., 2004. Climate controls on vegetation phenological patterns in northern mid- and high latitudes inferred from MODIS data. Glob. Chang. Biol. 10, 1133–1145.
Zhang, H.K., Roy, D.P., Yan, L., Li, Z., Huang, H., Vermote, E., Skakun, S., Roger, J.-C., 2018. Characterization of Sentinel-2A and Landsat-8 top of atmosphere, surface, and nadir BRDF adjusted reflectance and NDVI differences. Remote Sens. Environ. 215, 482–494.
Zhang, X., Xiao, X., Wang, X., Xu, X., Chen, B., Wang, J., Ma, J., Zhao, B., Li, B., 2020. Quantifying expansion and removal of Spartina alterniflora on Chongming island, China, using time series Landsat images during 1995-2018. Remote Sens. Environ. 247, 111916.
Zhong, L., Gong, P., Biging, G.S., 2014. Efficient corn and soybean mapping with temporal extendability: a multi-year experiment using Landsat imagery. Remote Sens. Environ. 140, 1–13.
Zuo, P., Zhao, S., Liu, C.A., Wang, C., Liang, Y., 2012. Distribution of Spartina spp. along China's coast. Ecol. Eng. 40, 160–166.